DELPHI Collaboration

DELPHI 2002-038 CONF 572
1 July, 2002

Search for Charged Higgs Bosons at LEP in general two higgs doublet models

M. Battaglia[1], J.Cuevas[2] M. Ellert[3], T. Ekelof[3], G. Gómez-Ceballos[4], A. Kiiskinen[5], P. Lutz[6] and F. Matorras[6]

[1]CERN, Geneva, Switzerland

[2]Dpto. Fisica, Univ. Oviedo, Spain

[3]Uppsala University, Uppsala, Sweden

[4]Instituto de Fisica de Cantabria (CSIC-UC), Santander, Spain

[5]Helsinki Institute of Physics, Helsinki, Finland

[6]CEA, Saclay, France

Abstract

A search for pair-produced charged Higgs bosons was performed in the high energy data collected by the DELPHI detector at LEP II at centre-of-mass energies from 183 GeV to 209 GeV. Five different final states, $\tau\nu\tau\nu$, $c\bar{s}\bar{c}s$, $c\bar{s}\tau\nu$, W^*AW^*A and $W^*A\tau\nu$ were considered, accounting for the major expected decays both in type I and type II two higgs doublet models. No excess of data compared to the expected Standard Model processes was observed and the existence of a charged Higgs boson with mass lower than 74.3 GeV/c^2 is excluded at the 95% confidence level, for any of the assumptions. Model independent cross section limits have also been calculated.

Contributed Paper for ICHEP 2002 (Amsterdam)

1 Introduction

A search for pair-produced charged Higgs bosons in e^+e^- collisions was performed using the data collected by DELPHI during the LEP runs at centre-of-mass energies from 189 GeV to 209 GeV. The results reported here update those obtained in an earlier analysis of the DELPHI data at lower centre-of-mass energies [1]. Similar searches have been performed by the other LEP experiments [2].

The existence of a pair of charged Higgs bosons is predicted by several extensions of the Standard Model. Pair-production of charged Higgs bosons occurs mainly via s-channel exchange of a photon or a Z^0 boson. In two Higgs doublet models (2HDM), the couplings are completely specified in terms of the electric charge and the weak mixing angle, θ_W, and therefore the production cross-section depends only on the charged Higgs boson mass. Higgs bosons couples to mass and therefore decay preferentially to heavy particles, but the precise branching ratios may vary significantly depending on the model. In most cases, for the masses at reach at LEP energies, the $\tau\nu_\tau$ and cs decay channels are expected to dominate. Analyses of the three possible final states, $\tau\nu\tau\nu$, $c\bar{s}c\bar{s}$ and $c\bar{s}\tau\nu$, have been performed and are described in this paper. To avoid loss of generality, the results are combined and interpreted treating the Higgs decay branching fraction to leptons as a free parameter. However, in type I models[1] and if the neutral pseudoscalar A is light (which is not excluded by direct searches for general 2HDM) the decay to W^*A can be predominant even in the range of masses of interest at LEP. Figs. 1 and 2 show the branching ratios for different parameters in this model [3]. To cover this eventuality the final states W^*AW^*A and $W^*A\tau\nu$ were also looked for. The channel W^*Acs is neglected because its contribution is expected to be very small. The results obtained for these channels are combined, together with those of the previous three channels and interpreted in this framework as a function of $\tan\beta$ with the expected branching ratios.

Different techniques were developed to improve the discrimination against the dominant W^+W^- background using multidimensional estimators based on discriminant variables such as the boson production angle, jet flavour tagging or τ polarisation.

2 Data sample

Data collected during the 2000 LEP run at centre-of-mass energies from 204 GeV to 208 GeV were used, with a total integrated luminosity of about 190 pb^{-1}. Approximately 60 pb^{-1} of this data was collected when one of the sectors of the TPC was unoperational (referred to as the S6 period in the following). The data collected during the years 1998 and 1999 at centre-of-mass energies from 189 GeV to 202 GeV were reanalysed, to take advantage of the improved performance on the reconstruction and selection. This additional data amounted to approximately 380 pb^{-1}.

The DELPHI detector and its performance have already been described in detail elsewhere [4, 5][2].

Signal samples were simulated using the HZHA generator [6]. The background estimates from the different Standard Model processes were based on the following event

[1] These are models where all fermions couple to the same Higgs doublet.

[2] The co-ordinate system used has the z-axis parallel to the electron beam, and the polar angle calculated with respect to this axis.

generators: KK2f [7] for $q\bar{q}(\gamma)$ and $\mu^+\mu^-$, KORALZ [9] $\tau^+\tau^-$, BHWIDE [10] for e^+e^- and WPHACT [11] for four-fermion final states. The four-fermion samples were complemented with two-photon interactions, generated with TWOGAM [12] for hadronic final states, BDK [13] for electron final states and BDKRC [13] for other leptonic final states. Both signal and background were generated for each of the centre-of-mass energies. A specific simulation, with the appropriate detector conditions, was performed for the S6 period.

3 Analysis

Most of the techniques and requirements follow closely those used for the WW selection [21], since the topology of the H^+H^- signal is very similar. We briefly describe them here together with other techniques specific to these analyses.

3.1 Run selection and track selection

To ensure a good detector performance the data corresponding to runs in which subdetectors were not fully operational were discarded. In particular it was required that the tracking subdetectors and calorimeters were fully operational. For all the topologies that involved leptons, it was further required that the muon chambers were active. This resulted in slightly smaller integrated luminosities than for the hadronic channel (see Tables 4 and 5).

Only charged tracks with an impact parameter in the transverse plane smaller than 5 cm, and with an axial coordinate $|z| < 10$ cm at the point of closest approach to the origin, was accepted. Tracks with a relative momentum error $\frac{\Delta p}{p} > 1$ were rejected.

Showers in the calorimeters were accepted as neutral particles if their energy was above 200 MeV.

3.2 Lepton identification

An isolated particle was identified as a muon if it gave signal in the muon chambers or left a signal in the calorimeters compatible with a MIP. It was identified as an electron if its energy deposition in the electromagnetic calorimeters was compatible with its measured momentum and the ionisation loss in the TPC was compatible with that expected from an electron of that momentum.

If an electron or muon had a momentum and energy deposition in the electromagnetic calorimeters smaller than $0.13\sqrt{s}$, it was assumed to come from τ decay and was therefore tagged as τ. In addition isolated jets with an energy of at least 5 GeV, at least one and at most five charged tracks and no more than ten particles in total were also considered as τ candidates.

For semileptonic final states tracks contained inside the jet, but forming an angle with jet axis of more than 15° were removed from the τ jet candidate. If the invariant mass of the jet was greater than 2.5 GeV/c^2, the tracks giving the greatest contribution to the mass (excluding the leading charged track in the jet) were excluded one by one in turn until the mass no longer exceeded 2.5 GeV. If more than one τ candidate was found they were selected with the following order of precedence: muon, electron, jet with lowest momentum weighted spread, single charged track.

The τ decays were classified into the following categories: e, μ, π, $\pi+n\gamma$, 3π according to the lepton identification, the number of charged tracks of the jet and the number of photons.

3.3 Tau polarisation

Assuming that the ν_τ has a definite helicity, the polarisation (P_τ) of tau leptons originating from heavy boson decays is determined entirely by the properties of weak interactions and the nature of the parent boson. The helicity configuration for the signal is $\mathrm{H}^- \to \tau_R^- \bar{\nu}_{\tau R}$ ($\mathrm{H}^+ \to \tau_L^+ \nu_{\tau L}$) and for the $\mathrm{W}^+\mathrm{W}^-$ background it is $\mathrm{W}^- \to \tau_L^- \bar{\nu}_{\tau R}$ ($\mathrm{W}^+ \to \tau_R^+ \nu_{\tau L}$) resulting in $P_\tau^{\mathrm{H}} = +1$ and $P_\tau^{\mathrm{W}} = -1$.

The τ weak decay induces a dependence of the angular and momentum distributions on polarisation. Once the τ decay channel is identified, the information on the τ polarisation was extracted from the observed kinematic distributions of its decay products, e.g. angles and momenta. These estimators are equivalent to those used at the Z peak for precision measurements [14]. For charged Higgs boson masses close to the threshold, the boost of the bosons is relatively small and the τ energies are similar to the τ's from Z decays at rest (40–50 GeV).

3.4 Jet definition and flavour tagging

The tracks were clustered into jets using the DURHAM[15] algorithm. For the *cscs* and W^*AW^*A the events, the jet algorithm was forced to produce a maximum of four jets. For the $cs\tau\nu$ and $W^*A\tau\nu$, the particles assigned to the tau candidate where excluded from this clustering and the remaining particles were forced into two jets. The 2 jets were required to have at least 1 charged track and 4 particles in total each.

In the *cscs* and $cs\tau\nu$ decay channels all four or both hadronic jets in the event originate from a c or s quark. In the hadronic background processes, such as $q\bar{q}$ and WW events, most or half of the jets have a different quark flavour or originate from a gluon. Therefore a jet flavour tagging algorithm was used as a tool in the analyses of the *cscs* and $cs\tau\nu$ channels. A similar jet flavour tagging technique has been used by DELPHI in a determination of $|V_{cs}|$ at LEP II [19].

This tagging was based on nine discriminating variables: three of them were related to the identified lepton and hadron content of the jet, two depended on kinematical variables and four on the reconstructed secondary decay structure. The finite lifetime of c (charm) particles was exploited to distinguish between c and light quark jets, while the c mass and decay multiplicity were used to discriminate against b jets. Furthermore s and c jets could be distinguished from u and d jets by the presence of an identified energetic kaon. Charged hadrons had been identified using the combined response of RICH and TPC dE/dx [20].

The responses of the flavour tagging algorithm for the individual jets were further combined into an event *cscs* probability or into a di-jet *cs* probability which were then used in background suppression.

3.5 Likelihood ratio techniques

In several of the analyses the final background discrimination was performed by using a likelihood ratio technique. Signal and background likelihoods, $\mathcal{L}_s$ and $\mathcal{L}_b$, were defined as products of the probability densities of the N discriminating variables, $\mathcal{L}_s = \prod_{i=1,N} s_i(x_i)$ and $\mathcal{L}_b = \prod_{i=1,N} b_i(x_i)$. For each of the measured values of the N discriminating variables, (x_i), the values of the signal and background probability densities, $s_i(x_i)$ and $b_i(x_i)$, were determined using samples of simulated signal and background events. The final event likelihood ratio, for simplicity referred to as "likelihood" in the following, was computed as a normalised ratio of the signal and background likelihoods, $\mathcal{L}_s/(\mathcal{L}_s + \mathcal{L}_b)$.

3.6 Mass reconstruction

The masses of the decaying bosons were reconstructed using a constrained fit requiring energy and momentum conservation with known beam energy (4-C fit). If the event was compatible with the hypothesis that the different objects were produced in the decay of two equal mass particles, an additional constraint was applied requiring that the two mass combinations were equal (5-C fit).

In the case of channels involving a $\tau\nu$ decay, the three components of the momentum vector of the ν_τ and the magnitude of the τ momentum were treated as free parameters, reducing the number of degrees of freedom of the fit from 5 to 1.

If two $\tau\nu$ decays were present, the number of unknowns was higher than the number of constraints and no mass could be estimated.

4 Selection

4.1 The $\tau\nu\tau\nu$ channel

The signature for $H^+H^- \to \tau^+\nu_\tau\tau^-\bar{\nu}_\tau$ is large missing energy and momentum and two acollinear and acoplanar[3] τ jets containing either a lepton or one or a few hadrons.

4.1.1 Event preselection

To select leptonic events a total charged particle multiplicity between 2 and 6 was required. Only events with two reconstructed jets both containing at least one charged particle and at least one of which contained only one charged particle were retained. It was also required that the angle between the two jets was larger than 30°.

Two-fermion and two-photon events were rejected by a requirement that the acoplanarity be larger than 13° if both jets were in the barrel region ($43° < \theta < 137°$) or larger than 25° otherwise.

The two-photon background was further reduced by different requirements on the jets: the sum of the jet energies transverse to the beam direction, $E_\perp$, was required to be greater than $0.1\sqrt{s}$; the total transverse momentum, $p_\perp$, to be greater than $0.04\sqrt{s}$; the total energy detected within 30° around the beam axis to be less than $0.1\sqrt{s}$; and the total energy outside this region to be greater than $0.1\sqrt{s}$.

[3]The acoplanarity is defined as the complement of the angle between the two jets projected onto the plane perpendicular to the beam.

To reject WW events where neither W decayed to $\tau\nu$, it was required that the two jets were identified as τ leptons. Events where the invariant mass of either of the jets was

4.1.2 Final background discrimination

Following the selection above most of the remaining background is $W^+W^- \to \tau^+\nu_\tau\tau^-\bar{\nu}_\tau$ events. Events from the H^+H^- signal and the W^+W^- background have similar topologies and due to the presence of missing neutrinos in the decay of each of the bosons it is not possible to reconstruct the boson mass. Two important differences, however, were used in order to discriminate the signal and the W^+W^- background: the boson polar angle and the τ polarisation.

A likelihood to separate the signal from the background was built using six variables: the estimators of the τ polarisation, the boson polar angle of both τ's, the acoplanarity and the total transverse momentum. The first two variables discriminated between $\tau\nu\tau\nu$ produced from W pairs or charged higgses pair. The last two variables had some sensitivity to the boson mass and helped in the discrimination of the remaining background from other processes. Some of these variables are shown in Fig. 3 and the resulting distribution of that likelihood for data, expected backgrounds and signal is shown in Fig. 4. The effects of the different sets of cuts are shown in Table 1 for the combined 183–209 GeV sample.

cut	data	total bkg.	4-fermion	other bkg.	ε_{80}
Leptonic selection	175699	176685.0	920.9	175764.1	72.22%
Acoplanarity cut	16607	16575.8	715.3	15860.5	62.27%
Energy/momentum cut	527	566.9	534.4	32.5	46.73%
τ identification	59	68.9	58.3	10.6	35.14%

Table 1: The total number of events observed and expected backgrounds in the $\tau\nu\tau\nu$ channel after the different cuts used in the analysis. The last column shows the efficiency for a charged Higgs boson signal with $m_{H^\pm} = 80$ GeV/c^2.

4.2 The *cscs* channel

In the analysis of the *cscs* channel both charged Higgs bosons are assumed to decay into a pair of c and s quarks producing a final state with four jets. The two dominant background sources of four-jet events are the $q\bar{q}gg$ background and fully hadronic four-fermion final states. The four-fermion background from WW production is much more severe than that from ZZ, because of the higher cross-section. Also, the same variables that are used for discrimination against the W^+W^- background usually work with similar efficiency against the Z^0Z^0 background. Therefore, the four-fermion sample is referred to as W^+W^- in the description of the analysis which follows.

4.2.1 Event preselection

In order to preselect hadronic events the following cuts were applied: the events had to contain at least 10 charged tracks, the visible energy of the reconstructed particles, E_{vis},

had to be larger than $0.6\sqrt{s}$, the reconstructed effective centre-of-mass energy, $\sqrt{s'}$, had to be larger than $0.85\sqrt{s}$. To reject hadronic back-to-back two-jet $q\bar{q}$ events the value of the thrust was required to be less than 0.95.

To select only true four-jet events it was imposed that the DURHAM clustering distance value for transition from four to three jets ($y_{4\to3}$) was greater than 0.002 and each jet was required to have at least three particles, out of which at least two charged, and a mass larger than 2 GeV/c^2. All jets were required to have energy above 5 GeV, and the minimum angle between any two jets was required to be at least 25°.

In order to obtain the best possible mass resolution a 5-C fit was performed for each of the three possible di-jet combinations, and the combination giving the smallest χ^2 was selected. An additional 4-C fit, imposing only energy-momentum conservation, was also performed and the difference between the masses of the two reconstructed bosons was calculated. The di-jet pairing used was the one giving the best 5-C fit. As the uncertainty of the di-jet mass reconstruction is approximately proportional to the mass, the boson mass difference of an event was scaled by dividing it by the 5-C fitted boson mass of the event in order to have a variable less dependent on the signal mass. This relative mass difference of the two reconstructed bosons was required to be below 25%.

After these selections the signal efficiency in the mass range of interest for this analysis was of the order of 70%.

4.2.2 Final background discrimination

Significant amounts of $q\bar{q}gg$ background still remained after the preselection. To suppress it further an anti-$q\bar{q}$ likelihood variable was constructed for additional $q\bar{q}$ background rejection.

The first of the variables used in the anti-$q\bar{q}$ likelihood, the event acoplanarity, separates signal and background using the differences in the event shape. The second one, the cosine of polar angle of the thrust axis, uses the fact that the signal events have uniform angular distribution whereas the jets in the $q\bar{q}$ background events are concentrated closer to the beam axis. The third variable is based on the fact that the probability of hard gluon radiation depends on the gluon energy and emission angle. Therefore the product of the minimum angle between two jets and the minimum jet energy in the event was used to separate between the signal and the $q\bar{q}gg$ events. The minimum energy and the minimum angle between jets are significantly different in signal events with low and high mass due to the large boost of light Higgs bosons. In order to reduce the mass dependence of the likelihood variables, the product of the minimum energy and the minimum angle was scaled by dividing it with the reconstructed Higgs boson mass of the event. The fourth variable used the fact that the charged Higgs bosons have equal mass whereas the masses of the di-jet pairs in the $q\bar{q}$ events are more or less randomly distributed. Therefore the relative mass difference, described in subsection 4.2.1, was a powerful discriminant variable. The last variable to be used in the likelihood was the output of the event *cscs*-tag, as all jets in the signal events originate from a c or s quark while this is true only for a fraction of the jets in the background. The normalised likelihood was required to exceed 0.3 to reject most of the $q\bar{q}$ background with a moderate signal efficiency loss.

Most of the background remaining after the anti-$q\bar{q}$ cut was hadronic decays of W pairs. A discriminant anti-WW likelihood was constructed for rejection of these events. If the mass of the charged Higgs boson coincides with the mass of the W boson the W^+W^-

background is partly irreducible. Some differences, however, exist and were used in order to discriminate between this difficult background and the signal.

The first of the variables in the anti-WW likelihood exploited the different polar angle distributions of the Higgs boson and the W boson, due to different spin properties This variable was the polar angle of the reconstructed positive boson where the charge was taken as the sum of the reconstructed momentum weighted charges of the two jets [18] used to reconstruct the boson. The boson with the higher value of charge was assumed to be the positive one and the other one was assumed to be the negative one. The second variable used for W^+W^- background discrimination was the *cs* event tag output which is useful as all signal jets originate from *c* and *s* quarks and only half of the background jets have the same quark flavours. The last variable used was the relative mass difference between the two reconstructed bosons. This variable has rejection power especially in cases where the reconstructed mass in W events is far away from the nominal W mass since in these events something has gone wrong in the jet momentum measurement, which usually leads to a higher mass difference between the reconstructed bosons. It also rejects more W^+W^- background than charged Higgs signal due to a larger natural width of the W boson. All events with anti-WW likelihood value below 0.4 were rejected.

The effects of the different sets of cuts are shown in Table 2 for the combined 183–209 GeV sample. The distribution of the anti-$q\bar{q}$ likelihood at the preselection level and the distribution of the anti-WW likelihood after a cut on the anti-$q\bar{q}$ likelihood are shown in Fig. 6. The reconstructed mass distribution for data, expected backgrounds and signal after the anti-$q\bar{q}$ and anti-WW cuts is shown in Fig. 7.

cut	data	total bkg.	4-fermion	other bkg.	ε_{75}	ε_{80}
4-jet presel.	5890	5902.5	4076.9	1825.6	83.0%	84.1%
Mass diff.	4326	4354.2	3389.6	964.6	71.0%	71.8%
anti-qq	2785	2808.1	2506.2	301.9	56.9%	57.8%
anti-WW	2114	2115.6	1855.5	260.1	52.8%	53.6%

Table 2: The total number of events observed and expected backgrounds in the *cscs* channel after the different cuts used in the analysis. The last columns shows the efficiencies for charged Higgs boson signals with $m_{H^\pm} = 75$ GeV/c^2 and $m_{H^\pm} = 80$ GeV/c^2, respectively.

4.3 The $cs\tau\nu$ channel

In the $cs\tau\nu$ channel one of the charged Higgs bosons decays into a $c\bar{s}$ quark pair, while the other decays into $\tau\nu_\tau$. Such an event is characterised by two hadronic jets, a τ candidate and missing energy carried by the neutrinos. The dominating background processes are $q\bar{q}g$ event production and semileptonic decays of W^+W^-. The same requirements for efficient operation of the most important sub-detectors were used as in the analysis of the leptonic channel.

4.3.1 Event preselection

An initial set of cuts was applied to reject purely leptonic events as well as two-photon interactions. The charged track multiplicity had to be at least 6 and the total momentum

of the charged tracks had to be greater than $0.01\sqrt{s}$. The quadratic sum of the forward and backward electromagnetic energies had to be less than $0.45\sqrt{s}$. The cosine of the polar angle of the missing momentum had to be less than 0.985 and the transverse energy had to be greater than $0.2\sqrt{s}$. The electromagnetic energy within a 15° cone around the beam-pipe was required to be less than 30 GeV.

To remove $q\bar{q}ll$ topologies, events with 2 or more leptons of the same flavour with momentum greater than $0.05\sqrt{s}$ and more than 10° isolation angle were rejected.

Another set of cuts was applied to reject the bulk of the $q\bar{q}\gamma$ radiative events. The cosine of the missing momentum had to be lower than 0.96, the difference between the centre-of-mass energy and the effective centre-of-mass energy ($\sqrt{s}-\sqrt{s'}$) had to be greater than 10 GeV, the visible energy had to be lower than $85\%\sqrt{s}$ and the DURHAM clustering distance when going from 4 to 3 jets ($y_{4\to3}$) if clustering all particles in the event had to be less than 0.03. The angle between the most energetic neutral particle in the event and the missing momentum had to be greater than 25°. If the cosine of the missing momentum was greater than 0.8, the effective centre-of-mass energy ($\sqrt{s'}$) had to be greater than 105 GeV and its difference to the centre-of-mass energy ($\sqrt{s}-\sqrt{s'}$) had to be greater than 25 GeV. If the angle between the two jets projected onto a plane perpendicular to the beam axis was greater than 165° then the angle between the plane spanned by the two jets and the tau candidate had to be greater than 7°.

Background from W^+W^- semileptonic decays not involving tau particles as well as a large fraction of the remaining $q\bar{q}$ was rejected by requiring the presence of a τ identified as described above. The momentum of the tau candidate had to be greater than 5 GeV and the product of the tau candidate momentum and its isolation angle had to be greater than 150 GeV·°. If the tau candidate contained more than 1 charged track, the cone around the jet axis containing 75% of the jet energy had to be smaller than 10°.

Finally, if the mass fit described above did not converge the event was rejected, reducing the background from misreconstructed WW pairs.

4.3.2 Final background discrimination

At this level of the selection there was still a very significant contribution of $q\bar{q}$ events. To further reject this background a likelihood function was defined. Different variables with important discrimination power were used. These were the event thrust, the cosine of the missing momentum, the angle between the two jets projected onto a plane perpendicular to the beam axis, the reconstructed polar angle of the negatively charged boson, the angle between the tau jet and the parent boson's momentum in the boson's rest-frame, the tau decay channel, the transverse momentum, $\sqrt{s'}/\sqrt{s}$, the angle between the plane spanned by the two jets and the tau candidate, the tau isolation angle and the DURHAM clustering distance when going from three to two jets ($y_{3\to2}$) if clustering all particles in the event. Some of these variables are shown in Fig. 8 and the result of the likelihood is shown in Fig. 9. Events with an anti-qq likelihood lower than 0.5 were rejected.

At this stage, most of the remaining background were W^+W^- with a semileptonic decay $q\bar{q}\tau\nu$, with topology equivalent to that of the charged higgs signal. Further background rejection was possible, however, using the tau polarisation and the cs quark flavour tag. Another likelihood function was therefore defined to discriminate between the remaining background and the expected signal using these two variables and some of the variables used in the previous anti-qq likelihood since these also contributed to the WW rejection.

The additional variables were the thrust, the angle between the two jets projected onto a plane perpendicular to the beam axis, the reconstructed polar angle of the negatively charged boson, the angle between the tau momentum and its parent boson's momentum in the boson's rest-frame and the tau isolation angle. Some of these variables are shown in Fig. 8 and the result of the likelihood is shown in Fig. 9. No cut was made on this function, but it was used in the limit estimation as described below.

cut	data	total bkg.	4-fermion	other bkg.	ε_{75}
Preselection	31138	29803.1	9449.0	20354.1	95.8%
Bulk $q\bar{q}$ rejection	6267	5899.7	3939.7	1960.0	84.9%
$qq\tau\nu$ selection	3054	2814.5	1649.0	1165.4	66.1%
anti-qq likelihood > 0.5	1085	1081.7	985.3	95.9	57.5%

Table 3: The number of events selected in the data and expected from Monte Carlo after the different cuts in the $cs\tau\nu$ analysis. The number of events correspond to the full data set (1998–2000). The efficiency in the last column correspond to a charged Higgs boson with a mass of 75 GeV/c^2.

4.4 Channels including a W^*A decay

If at least one of the Higgs bosons decays to a W^*A pair, there are several possible topologies depending on the different boson decays. The W can decay leptonically or hadronically, and the number of jets strongly depends on the A mass and on the boson boosts. To treat all these decays in a generic way, the search was restricted to A masses above 12 GeV, where it decays predominantly to $b\bar{b}$ and an inclusive search is performed. Events with jets with b quark content were searched for in two topologies:

- events with a τ, missing energy and at least two hadronic jets
- events with no missing energy and at least four hadronic jets

No constraint on the maximum number of jets was adopted. In this way most of the possible decay chains for the $W^*A\tau\nu$ (first topology) and W^*AW^*A (second) were covered. The decay to W^*Acs was neglected because its contribution is very small for all values of the model parameters.

It was found that the analysis designed by DELPHI for technicolor search[22] was well suited also for these topologies and had a good performance on this search. It was therefore adopted here. Fig. 11 shows the reconstructed mass of the selected candidates.

5 Systematic errors

Uncertainties in the expected background and in the signal efficiency were accounted for at each centre-of-mass energy and separately for the S6 period. Small contributions to these uncertainties are due to uncertainties in the luminosity measurement and in the cross-section estimates for the simulated data samples. The systematic error estimation for the background follows closely the treatment in the DELPHI W^+W^- analysis [21].

The largest part of the background and signal efficiency uncertainties in the $\tau\nu\tau\nu$ channel is due to the limited simulation statistics available. Several additional sources of systematic uncertainties were investigated. In particular, the track reconstruction efficiency, the τ identification and the behaviour of different variables were studied. The lepton identification was checked with di-lepton samples selected by kinematic cuts and without particle identification requirements. Data at the Z peak and at high energy were used. Monte Carlo predictions were found to agree with the data measurements within the statistical errors (about 1%). The same leptonic samples were used to check the track reconstruction efficiency on isolated particles, showing agreement at the 1% level. This error was taken as an estimate of the contribution to the systematic error both for signal and background, since the dominant background at final selection level has a topology very similar to that of the signal. The modelling of the preselection variables agrees within statistical errors with the data. The momentum and electromagnetic energy scales and resolutions were investigated using $\mu^+\mu^-\gamma$ or $e^+e^-\gamma$ data and simulated test samples. The variation was negligible for both signal- and background rates. Additional systematic effects were estimated by comparing the data collected at the Z peak during the period when sector 6 of the TPC was not functioning with simulation samples produced with the same detectors conditions. This did not give any significant increase, compared to the numbers above. The total systematic error on the signal efficiency was 2% and the total relative systematic error on the background rate was 10%.

In the *cscs* analysis the two background sources were the $q\bar{q}gg$ background and fully hadronic four-fermion final states.

The total uncertainty of the $q\bar{q}gg$ background estimate at the four-jet preselection level is the combination of the uncertainties in the integrated luminosity, in the uncertainty of the cross-section of that process and in the possible differences between the real data and the physics and detector simulation of the $q\bar{q}gg$ background. These effects have been studied in detail in [21] where the largest contribution of the selection uncertainty in a similar four-jet selection was found to be due to the hadronisation model and imperfections in the generator model. Based on a comparison of two models, JETSET 7.4 and ARIADNE, the total uncertainty of the $q\bar{q}gg$ event rate in the four-jet event sample was estimated to be of the order of 5%.

Similarly, a part of the uncertainty in the fully hadronic four-fermion background (mainly WW), is due to the uncertainties in the luminosity measurement and in the cross-section estimate. The precision of the Standard Model prediction for the WW production cross-section estimate depends on the centre-of-mass energy and has been estimated to be of the order of 1%. As the four-jet event selection of the DELPHI WW cross-section measurement is quite similar to the preselection used here, the uncertainty in the preselection efficiency was taken to be similar to the corresponding analysis of that analysis [21] which has been studied in detail and found to be 0.6%. The main contributions to this uncertainty also arise from the hadronisation model with smaller contributions from the detector simulations. Combining these uncertainties the estimated precision of the four-fermion background rate at the preselection level was 1.3%.

Further systematic effects could have been introduced in the analysis when applying the relative mass difference cut and the likelihood background rejections. Any potential differences in the shapes of these variables between the data and the simulations would affect the efficiency of the cuts. Comparisons between real and simulated date were made at early selection levels in order to keep the event rates reasonably high, enabling large

statistics for the comparisons and keeping the signal-to-background rate so small that a possible signal in the data would not affect the distributions significantly. The uncertainty of the background rate due to the relative mass difference cut was estimated to be 1%. The effect of potential systematic effects of the shapes of the likelihood variable distributions was studied by changing the variable shapes in the simulation by reweighting simulated events. The reweighted events were propagated through the analysis and the effect on the cut efficiencies was studied. The uncertainty of the anti-qq likelihood and anti-WW cuts were estimated to be 2.3% and 0.7%. Uncertainties in the final discriminating likelihood shape, which would affect the signal likelihood of the data events, were also taken into account. A change in the likelihood shape would influence the likelihood ratio in the exclusion limit calculation. This effect was taken into account by increasing the background rate uncertainty by an additional 2%.

Combination of all background uncertainties leads to a total uncertainty of 4% in the background normalisation. The uncertainty of the signal efficiency was estimated to be 2.5% with a 1% contribution from beam energy, hadronisation model etc., a 1.2% contribution from limited simulation statistics and a 2% contribution from the cuts and likelihoods.

Also in the $cs\tau\nu$ there was a contribution to the systematic error from the uncertainties in the qq and WW total normalisation, estimated as for $cscs$ to be 0.4% and 0.9%, respectively. The isolated lepton identification efficiency contributed with 1% both to the signal and background systematics. The uncertainties of the selection variables were estimated by comparing the shapes of the variable distributions in data and simulation at the preselection level. The agreement of all variables was found to be satisfactory. Nevertheless, the potential error was estimated conservatively from the observed difference between real data and simulation when any particular cut was varied within the resolution of that variable. Combining these errors, a total uncertainty of 2.4% was estimated for the background rate and 0.3% in the signal efficiency. For the likelihoods, the reweighting procedure described for $cscs$ was followed, estimating the total contribution to 7.6% for the background and 3.2% for the signal.

For the $W^*A\tau\nu$ and the W^*AW^*A channels, the systematic studies are described in detail in [22]. The errors were studied in a similar way to the ones described above with an additional contribution from the b-tagging and with the difference that the WW is not the dominant background. The total systematics on the signal efficiency for the W^*AW^*A and $W^*A\tau\nu$ were 5% and 2% respectively. The relative error on the background were 11% and 10%.

6 Results

The number of real data and background events and the estimated efficiencies for these selections for different $H^{\pm}$ masses are summarised in Tables 4 and 5. The quoted errors include the systematic uncertainties in the expected background and the signal efficiency.

6.1 Determination of the mass limit

No significant signal-like excess of events compared to the expected backgrounds was observed in any of the five final states investigated. A lower limit for a charged Higgs

Chan.	$\sqrt{s}$	lum.	data	total bkg.	ε_{75}	ε_{80}
$\tau\nu\tau\nu$	189	153.8	14	17.8± 1.4	35.2±1.5%	35.7±1.5%
$\tau\nu\tau\nu$	192	24.5	3	2.9± 0.2	33.6±1.5%	37.0±1.5%
$\tau\nu\tau\nu$	196	72.4	10	9.1± 0.7	33.6±1.5%	37.0±1.5%
$\tau\nu\tau\nu$	200	81.8	10	9.7± 0.8	32.3±1.5%	35.5±1.5%
$\tau\nu\tau\nu$	202	39.4	2	4.7± 0.4	32.3±1.5%	35.5±1.5%
$\tau\nu\tau\nu$	205	69.1	10	8.5± 0.6	32.2±1.5%	33.4±1.5%
$\tau\nu\tau\nu$	206.6	79.8	5	10.1± 0.8	32.2±1.5%	33.4±1.5%
$\tau\nu\tau\nu$	206.3(S6)	50.0	5	6.1± 0.5	31.7±1.5%	35.7±1.5%
$cscs$	189	158.0	565	554.9±22.2	52.1±1.3%	52.6±1.3%
$cscs$	192	25.9	90	93.1± 3.7	54.6±1.4%	54.1±1.4%
$cscs$	196	76.9	284	279.7±11.2	54.6±1.4%	54.1±1.4%
$cscs$	200	84.3	299	300.6±12.2	53.1±1.3%	53.9±1.3%
$cscs$	202	41.1	147	136.5± 5.5	53.1±1.3%	53.9±1.3%
$cscs$	205	75.6	270	264.5±10.6	51.5±1.3%	53.6±1.3%
$cscs$	206.6	87.8	291	288.3±11.5	52.1±1.3%	53.5±1.3%
$cscs$	206.3 (S6)	60.8	168	196.9± 7.9	51.5±1.3%	53.6±1.3%
$cs\tau\nu$	189	153.8	296	285.8±22.9	57.5±2.7%	57.1±2.7%
$cs\tau\nu$	192	24.5	56	47.5± 3.8	57.6±2.7%	56.5±2.7%
$cs\tau\nu$	196	72.4	147	143.8±11.5	57.6±2.7%	56.5±2.7%
$cs\tau\nu$	200	81.8	158	154.6±12.4	57.4±2.7%	57.3±2.7%
$cs\tau\nu$	202	39.4	71	75.7± 6.1	57.4±2.7%	57.3±2.7%
$cs\tau\nu$	205	69.1	130	129.5±10.4	57.2±2.7%	55.5±2.6%
$cs\tau\nu$	206.6	79.8	139	150.4±12.0	57.2±2.7%	55.5±2.6%
$cs\tau\nu$	206.3(S6)	50.0	88	94.4± 7.6	57.7±2.7%	55.9±2.6%

Table 4: Integrated luminosity, observed number of events, expected number of background events and signal efficiency (75 GeV/c^2 and 80 GeV/c^2 masses) for different decay channels and centre-of-mass energies.

boson mass was derived at 95% confidence level in two scenarios. In the first scenario it was assumed that the charged Higgs boson decayed in 100% of the cases to either $\tau\nu$ or cs. The limits were extracted as a function of the leptonic Higgs decay branching ratio BR(H $\rightarrow \tau\nu_\tau$). In the second scenario the WA decay was allowed and limits were computed for different values of M_A as a function of $\tan\beta$. The branching ratios were calculated according to [3] as a function of $\tan\beta$, the centre-of-mass energy and the neutral pseudoscalar and charged higgs masses.

In both cases, the confidence in the signal hypothesis, CL_s, was calculated using a likelihood ratio technique [23].

The background and signal probability density functions of one or two discriminating variables in each channel were used. The data samples collected at the different centre-of-mass energies were treated separately and combined as individual experiments. In the $cscs$ and $cs\tau\nu$ channels the two discriminating variables were the reconstructed mass and the anti-WW likelihood, in the W^*AW^*A and $W^*A\tau\nu$ the likelihood was replaced by the final neural network output. In the $\tau\nu\tau\nu$ channel only the background discrimination likelihood was used since mass reconstruction is not possible. The distributions of the

Chan.	$\sqrt{s}$	lum.	data	total bkg.	ε_{80}	ε_{90}
$WA\tau\nu$	189	153.8	12	11.4± 0.7	20.5±2.2%	10.2±2.1%
$WA\tau\nu$	192	24.5	3	1.6± 0.1	20.1±2.2%	11.4±2.1%
$WA\tau\nu$	196	72.4	2	4.7± 0.3	20.1±2.2%	11.4±2.1%
$WA\tau\nu$	200	81.8	4	4.9± 0.3	21.0±2.2%	13.7±2.1%
$WA\tau\nu$	202	39.4	4	2.5± 0.2	21.0±2.2%	13.7±2.1%
$WA\tau\nu$	205	69.1	4	4.1± 0.2	21.3±2.2%	15.5±2.2%
$WA\tau\nu$	206.6	79.8	6	4.6± 0.3	21.3±2.2%	15.5±2.2%
$WA\tau\nu$	206.3(S6)	50.0	4	3.0± 0.2	21.3±2.2%	15.5±2.2%
$WAWA$	189	158.0	81	79.7± 7.9	35.6±5.1%	39.4±5.1%
$WAWA$	192	25.9	16	13.0± 1.3	35.6±5.1%	39.4±5.1%
$WAWA$	196	76.9	37	35.3± 3.5	35.6±5.1%	39.4±5.1%
$WAWA$	200	84.3	36	35.6± 3.6	35.5±5.1%	39.3±5.1%
$WAWA$	202	41.1	16	17.7± 1.8	35.5±5.1%	39.3±5.1%
$WAWA$	205	75.6	24	24.7± 2.5	37.8±5.1%	34.5±5.1%
$WAWA$	206.6	87.8	30	28.3± 2.8	37.8±5.1%	34.5±5.1%
$WAWA$	206.3(S6)	60.8	13	18.2± 2.8	37.8±5.1%	34.5±5.1%

Table 5: Integrated luminosity, observed number of events, expected number of background events and signal efficiency (80 GeV/c^2 and 90 GeV/c^2 charged Higgs masses, and M_A=12 GeV/c^2) for different WA decay channels and centre-of-mass energies.

discriminating variable for signal events, obtained by the simulation at different $H^{\pm}$ mass values for each $\sqrt{s}$, were interpolated for intermediate mass values.

The estimated uncertainties on background and signal were taken into account in the limit derivation by a Gaussian smearing of the central values of the number of expected events.

The resulting limits at 95% confidence level are shown in Figs. 12 and 14 for the two scenarios as functions of the leptonic branching ratio and $\tan\beta$, respectively. The expected median [4] of the lower mass limits has been obtained from a large number of simulated experiments. Figures 13 and 15 show the obtained and expected confidence levels for the background only hypothesis, showing a good agreement.

If the W^*A decay is forbidden, a lower $H^{\pm}$ mass limit of $M_{H^{\pm}} > 74.3$ GeV/c^2 can be set at the 95% confidence level, independently of the branching ratio BR($H \to \tau\nu_\tau$). The median of the limits is 76.4 GeV/c^2. The noticeable difference between observed and expected limit is dominated by a small "hole" around BR=0.35 which reaches only 92% as confidence level, produced by a small excess of data in that region in the semileptonic channel.

If the W^*A decay is allowed, a lower $H^{\pm}$ mass limit of $M_{H^{\pm}} > 76.7$ GeV/c^2 can be set at the 95% confidence level, independently of $\tan\beta$ for $M_A > 12$. The median of the limits obtained from a large number of simulated Gedanken experiments is 77.9 GeV/c^2. Table 6 show the limits obtained for different values of M_A and $\tan\beta$.

[4]The median is calculated as the value which has 50% of the limits of the simulated experiments below it and similarly, the $\pm$ 1σ estimations correspond to 84% and 16% of the simulated experiments.

M_A	$\tan\beta = 0.01$	$\tan\beta = 100$	minimum
12	81.4 (80.3)	81.5 (82.9)	76.7 (77.9)
30	81.4 (80.4)	84.1 (86.0)	77.7 (78.3)
50	81.6 (80.3)	87.7 (89.0)	79.4 (79.1)
70	81.7 (80.3)	87.4 (88.6)	80.0 (79.4)

Table 6: Observed limits at 95% C.L. for different values of M_A and $\tan\beta$. The expected median limit is shown in parenthesis. The second column shows the limit for small values of $\tan\beta$, the third the limits when $\tan\beta$ is high and the last column shows the worst limit for any $\tan\beta$ for a given M_A.

6.2 Cross section limit

The results are also expressed as 95% confidence level upper limits for the charged Higgs boson production cross-section as a function of the charged Higgs boson mass, for different assumptions on the model parameters, *i.e.* leptonic branching ratio for the first scenario and M_A and $\tan\beta$ for the second. These cross-section limits were determined for each mass point by scaling the expected 2HDM signal cross-section up or down until the confidence level of exclusion reached 95%, therefore the only assumption taken from the model is the dependence of the cross section on the mass and centre-of-mass energy and thus this approach can be considered model independent. Results are summarised in Figs. 16 and 17. The excluded cross-sections are given for 206.3 GeV centre-of-mass energy.

7 Conclusion

A search for pair-produced charged Higgs bosons was performed using the full statistics collected by DELPHI at LEP at centre-of-mass energies from 189 GeV to 209 GeV searching for the $\tau\nu\tau\nu$, $cscs$, $cs\tau\nu$, W^*AW^*A and $W^*A\tau\nu$ final states. No significant excess of candidates was observed and lower limits on the charged Higgs mass were set in two frameworks. Assuming that the branching ratio to WA is negligible (type II models or type I with a heavy neutral pseudoscalar) limits are set at 95% confidence level as a function of the branching ratio to leptons. Results are shown in Figs. 12 and 14. The absolute limit is 74.3 GeV at 95%. Limits were also set within type I models for different M_A from 12 GeV to 80 GeV as a function of $\tan\beta$. Results are shown in Figs. 16 and 17. The absolute limit is 76.7 GeV at 95%.

To allow a less model dependent comparison limits are also expressed in terms of upper bounds in the cross section for different sets of the model parameters. Results are shown in Figs. 16 and 17

This analysis improves previous searches both by the inclusion of new discriminant techniques and by the less model dependent approach allowing more sensitivity and covering a wider range of models and model parameters.

Acknowledgements

We are greatly indebted to our technical collaborators, to the members of the CERN-SL Division for the excellent performance of the LEP collider, and to the funding agencies for their support in building and operating the DELPHI detector.
We acknowledge in particular the support of
Austrian Federal Ministry of Science and Traffics, GZ 616.364/2-III/2a/98,
FNRS–FWO, Belgium,
FINEP, CNPq, CAPES, FUJB and FAPERJ, Brazil,
Czech Ministry of Industry and Trade, GA CR 202/96/0450 and GA AVCR A1010521,
Danish Natural Research Council,
Commission of the European Communities (DG XII),
Direction des Sciences de la Matière, CEA, France,
Bundesministerium für Bildung, Wissenschaft, Forschung und Technologie, Germany,
General Secretariat for Research and Technology, Greece,
National Science Foundation (NWO) and Foundation for Research on Matter (FOM), The Netherlands,
Norwegian Research Council,
State Committee for Scientific Research, Poland, 2P03B06015, 2P03B1116 and SPUB/P03/178/98,
JNICT–Junta Nacional de Investigação Científica e Tecnológica, Portugal,
Vedecka grantova agentura MS SR, Slovakia, Nr. 95/5195/134,
Ministry of Science and Technology of the Republic of Slovenia,
CICYT, Spain, AEN96–1661 and AEN96-1681,
The Swedish Natural Science Research Council,
Particle Physics and Astronomy Research Council, UK,
Department of Energy, USA, DE–FG02–94ER40817.

References

[1] P. Abreu *et al.* (DELPHI Collaboration), Phys. Lett. **B 525** (2002) 17.
P. Abreu *et al.* (DELPHI Collaboration), Phys. Lett. **B 460** (1999) 484.

[2] R. Barate *et al.* (ALEPH Collaboration), Phys. Lett. **B 487** (2000) 253.
M. Acciarri *et al.* (L3 Collaboration), Phys. Lett. **B 496** (2000) 34.
G. Abbiendi *et al.* (OPAL Collaboration), Eur. Phys. J. **C 7** (1999) 407.

[3] A.G. Akeroyd *et al.*Eur. Phys. J. **C 20** (2001) 51.

[4] P. Aarnio *et al.* (DELPHI Collaboration), Nucl. Instr. and Meth. **A 303** (1991) 233.

[5] P. Abreu *et al.* (DELPHI Collaboration), Nucl. Instr. and Meth. **A 378** (1996) 57.

[6] P. Janot, in CERN report 96-01, Vol. 2, p. 309.

[7] S. Jadach, B.F.L. Ward, Z. Was, Phys. Lett. **B449** (1999) 97;

[8] T. Sjöstrand, Comp. Phys. Comm. **82** (1994) 74.

[9] S. Jadach, B.F.L. Ward, Z. Was, Comp. Phys. Comm. **79** (1994) 503.

[10] S. Jadach, W. Placzek, B.F.L. Ward, Comp. Phys. Comm. **79** (1994) 503.

[11] E. Accomando and A. Ballestrero, Comp. Phys. Comm. **99** (1997) 270.

[12] S. Nova, A. Olchevski and T. Todorov, in CERN Report 96-01, Vol. 2. p. 224.
T. Alderweireld *et al.*, in CERN Report 2000-009, p. 219.

[13] F.A. Berends, P.H. Daverveldt, R. Kleiss, Comp. Phys. Comm. **40** (1986) 271, 285 and 309.

[14] P. Abreu *et al.* (DELPHI Collaboration), Zeit. Phys. **C 67** (1995) 183.

[15] S. Catani *et al.*, Phys. Lett. **B 269** (1991) 432.

[16] P. Abreu *et al.* (DELPHI Collaboration), Eur. Phys. J. **C 10** (1999) 563.

[17] E. Norrbin and T. Sjöstrand, Phys. ReV. **D 55** (1997) 55.

[18] P. Abreu *et al.* (DELPHI Collaboration), Phys. Lett. **B 502** (2001) 9.

[19] P. Abreu *et al.* (DELPHI Collaboration), Phys. Lett. **B 439** (1998) 209.

[20] M. Battaglia and P. M. Kluit, Nucl. Instr. and Meth. **A 433** (1999) 252.

[21] P. Abreu *et al.* (DELPHI Collaboration), Phys. Lett. **B 479** (2000) 89.
P. Abreu *et al.* (DELPHI Collaboration), new paper?.

[22] P. Abreu *et al.* (DELPHI Collaboration), Eur.Phys.J. **C 22** (2001) 17.

[23] A.L. Read, in CERN report 2000-005, p. 81

[24] ALEPH, DELPHI, L3 and OPAL Collaborations, *Searches for Higgs bosons: Preliminary combined results using LEP data collected at energies up to 202 GeV*, CERN-EP 2000-055.

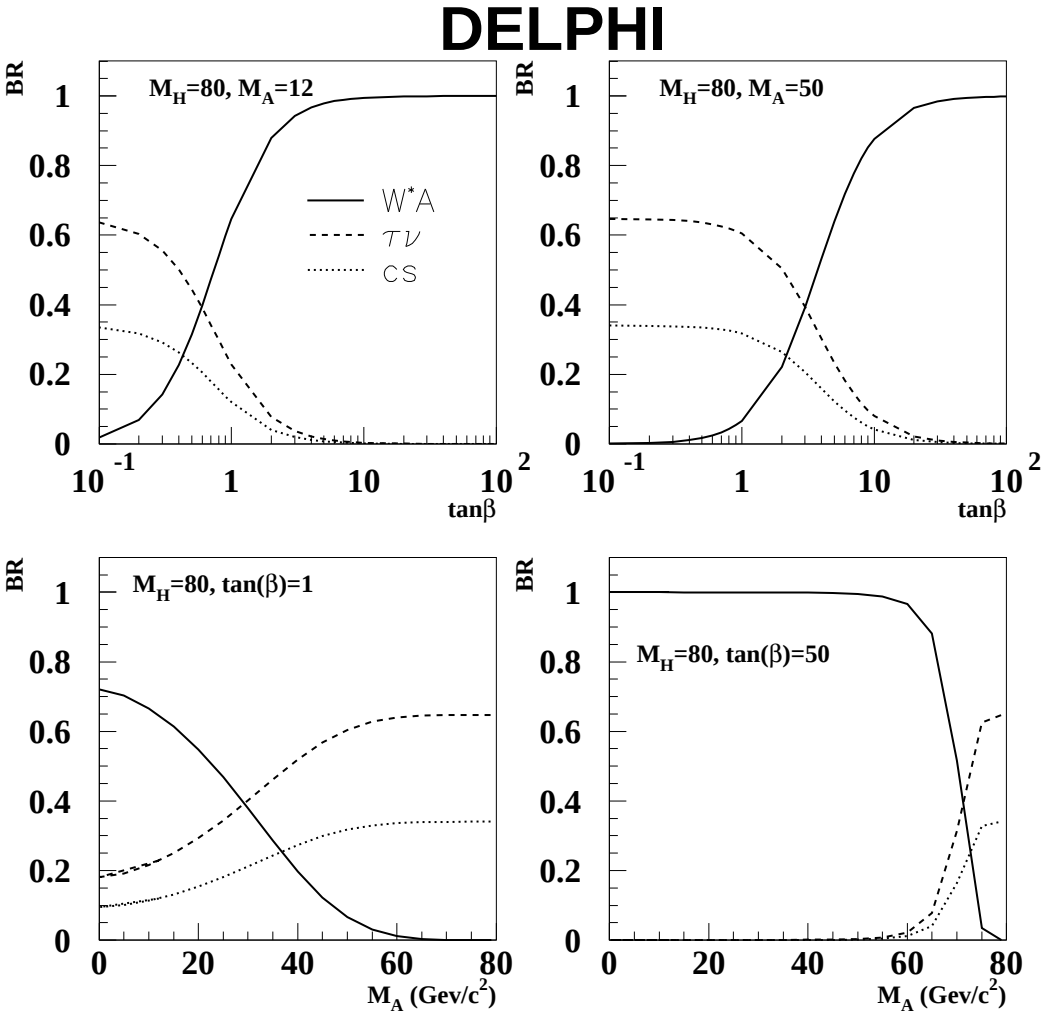

Figure 1: Predicted charged higgs decay branching ratios for different parameters.

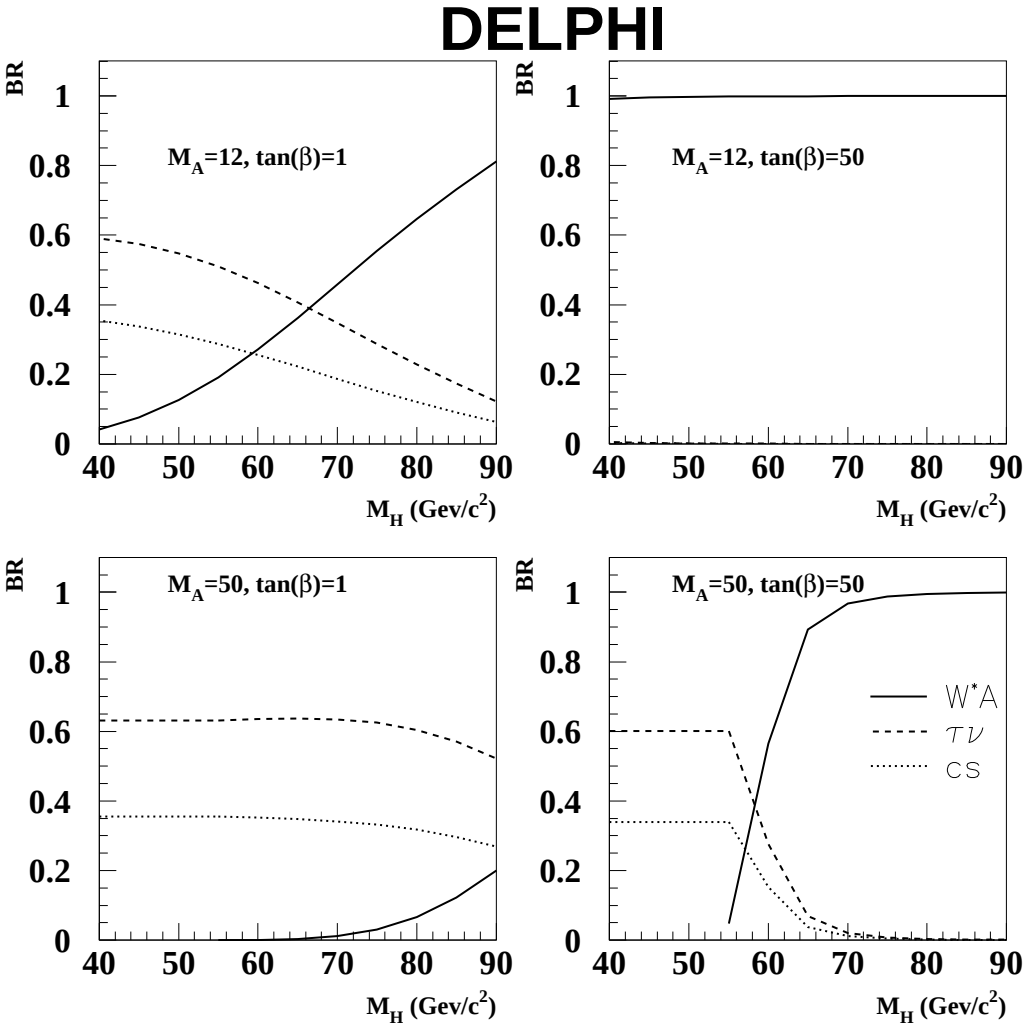

Figure 2: Predicted charged higgs decay branching ratios for different parameters.

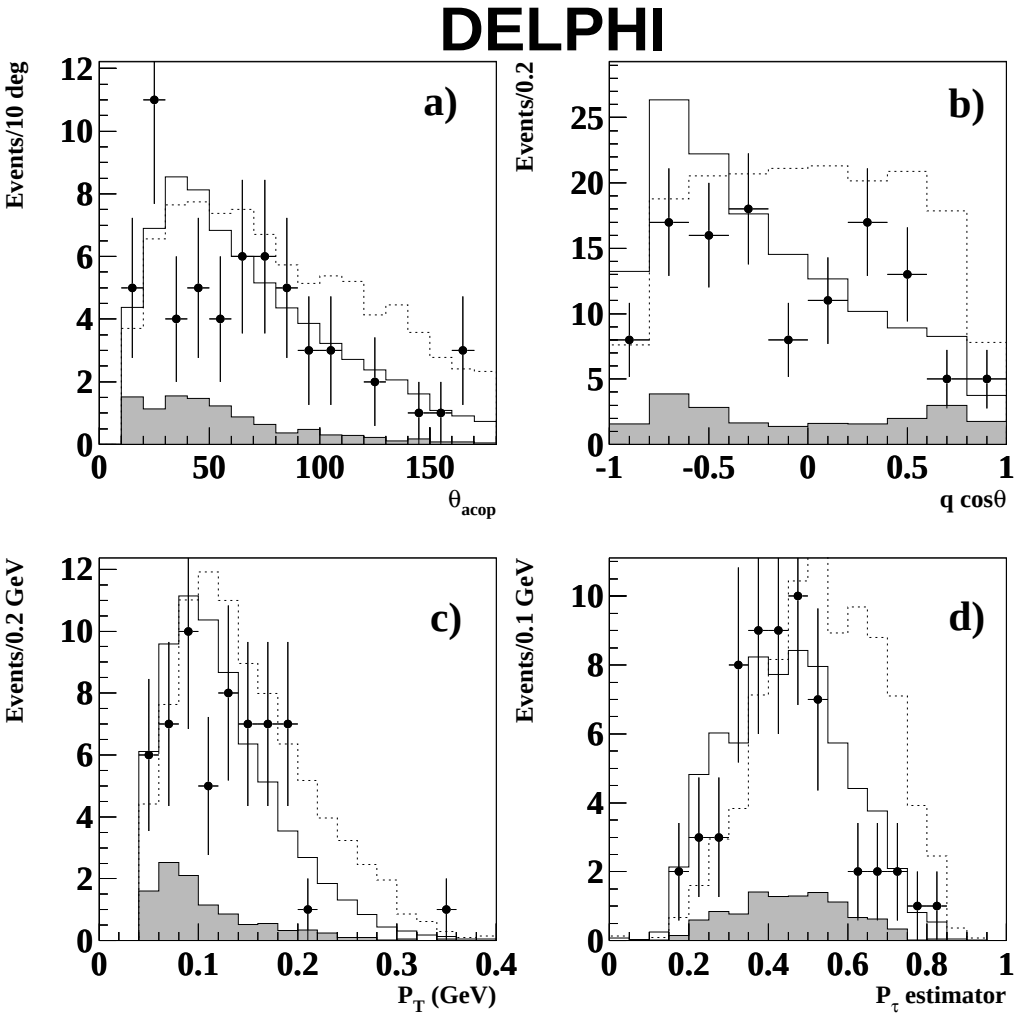

Figure 3: Distribution of some of the variables used for the anti-WW likelihood for the $\tau\nu\tau\nu$ analysis at 189–209 GeV after preselection: a) acoplanarity, b) cosine of polar angle accounting for the charge, c) transverse momentum and d) τ polarisation estimator. Data are shown as filled circles, while the solid histogram contour shows the expected SM background with contributions from WW (unfilled) and $q\bar{q}$ (shaded). The expected histogram for a 85 GeV/c^2 charged Higgs boson signal is shown as a dashed line in arbitrary normalisation for comparison.

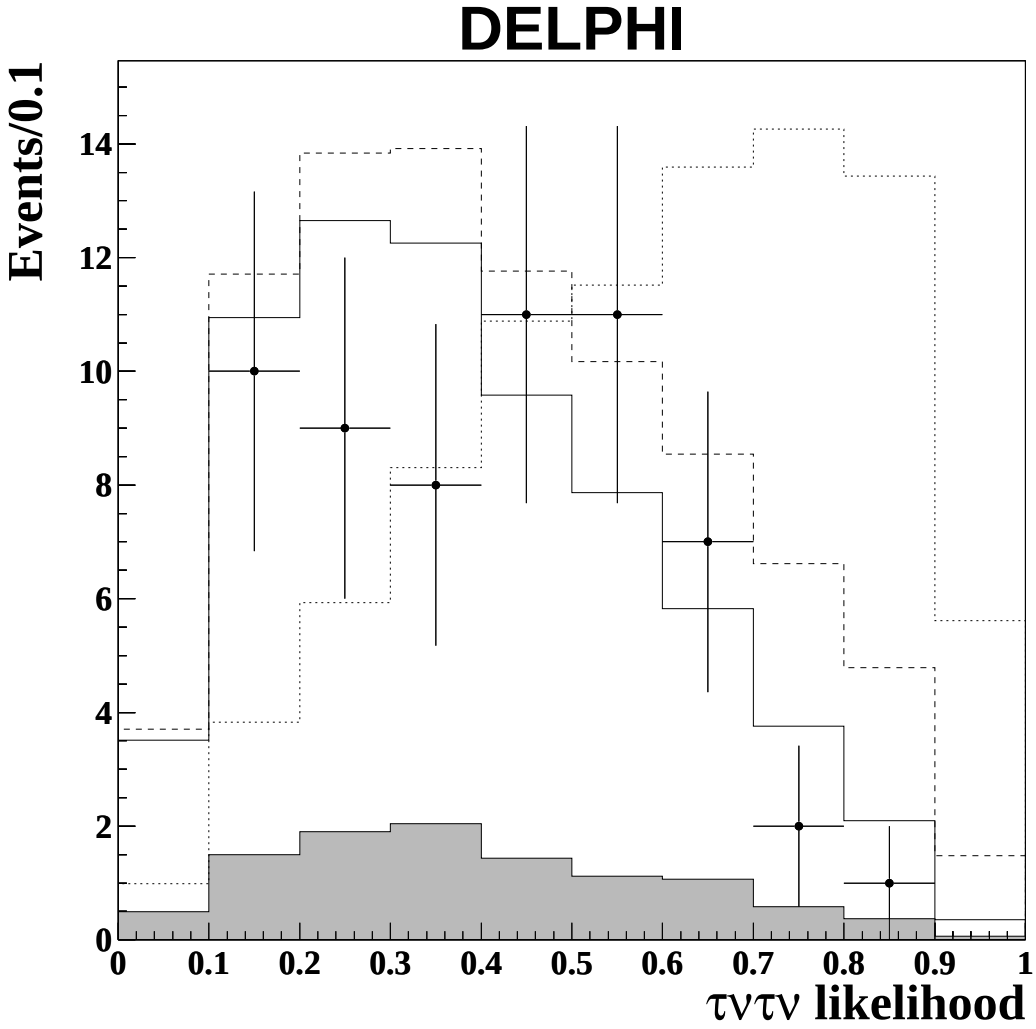

Figure 4: Distribution of the anti-WW likelihood for the $\tau\nu\tau\nu$ analysis at 189–209 GeV. The dots represent the data, while the solid histogram contour shows the expectation from SM processes, as in figure 3. The expected histogram for a 85 GeV/c^2 charged Higgs boson signal has been normalised to the production cross-section and 100% leptonic branching ratio and added to the backgrounds (dashed). The dotted line shows the shape of the likelihood for the charged higgs signal only in arbitrary normalization.

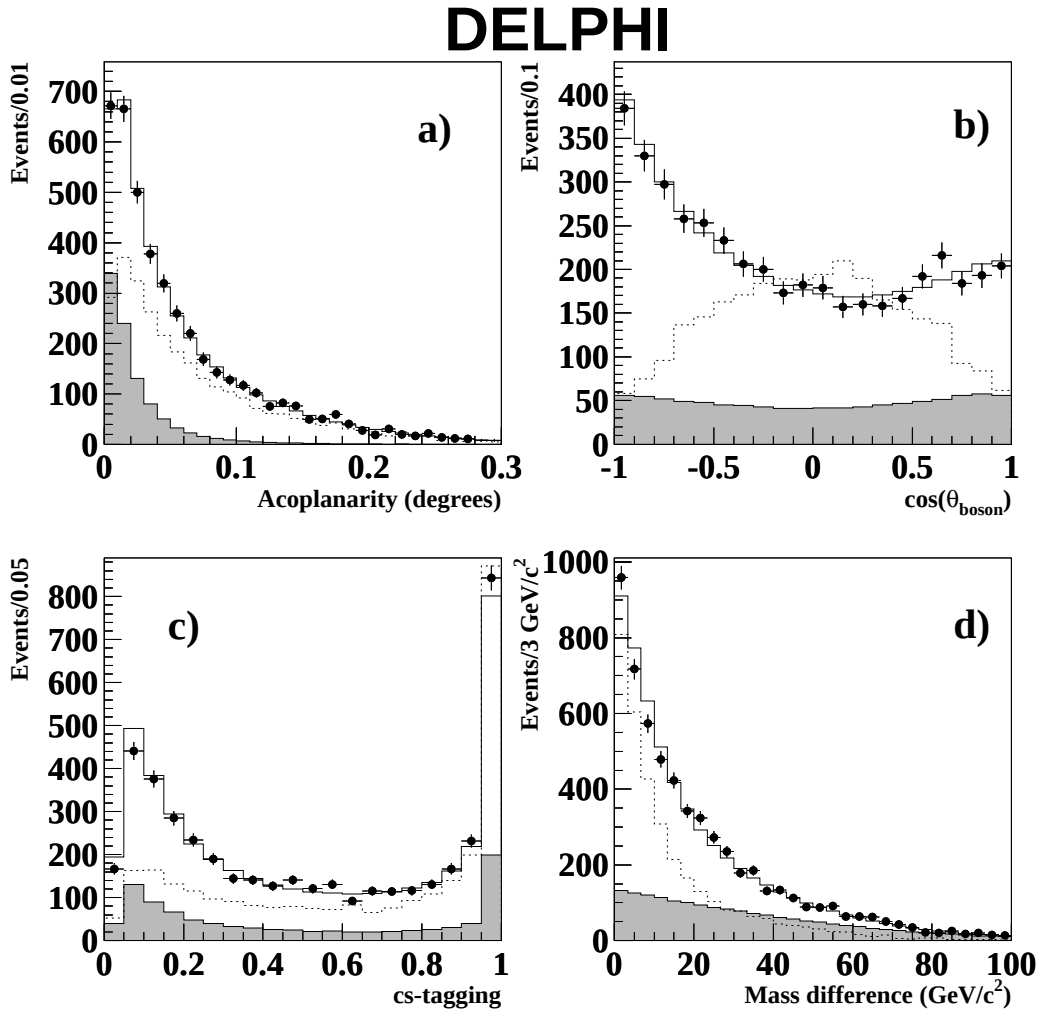

Figure 5: Distribution of some of the variables used for the anti-qq and anti-WW likelihoods in the *cscs* analysis at 189–209 GeV after preselection: a) acoplanarity, b) signed polar angle of the boson c)cs-tagging variable and d)mass difference. Data are shown as filled circles, while the solid histogram contour shows the expected SM background with contributions from WW (unfilled) and $q\bar{q}$ (shaded). The expected distribution for a 75 GeV/c^2 charged Higgs boson signal is shown as a dotted histogram with arbitrary normalisation for comparison.

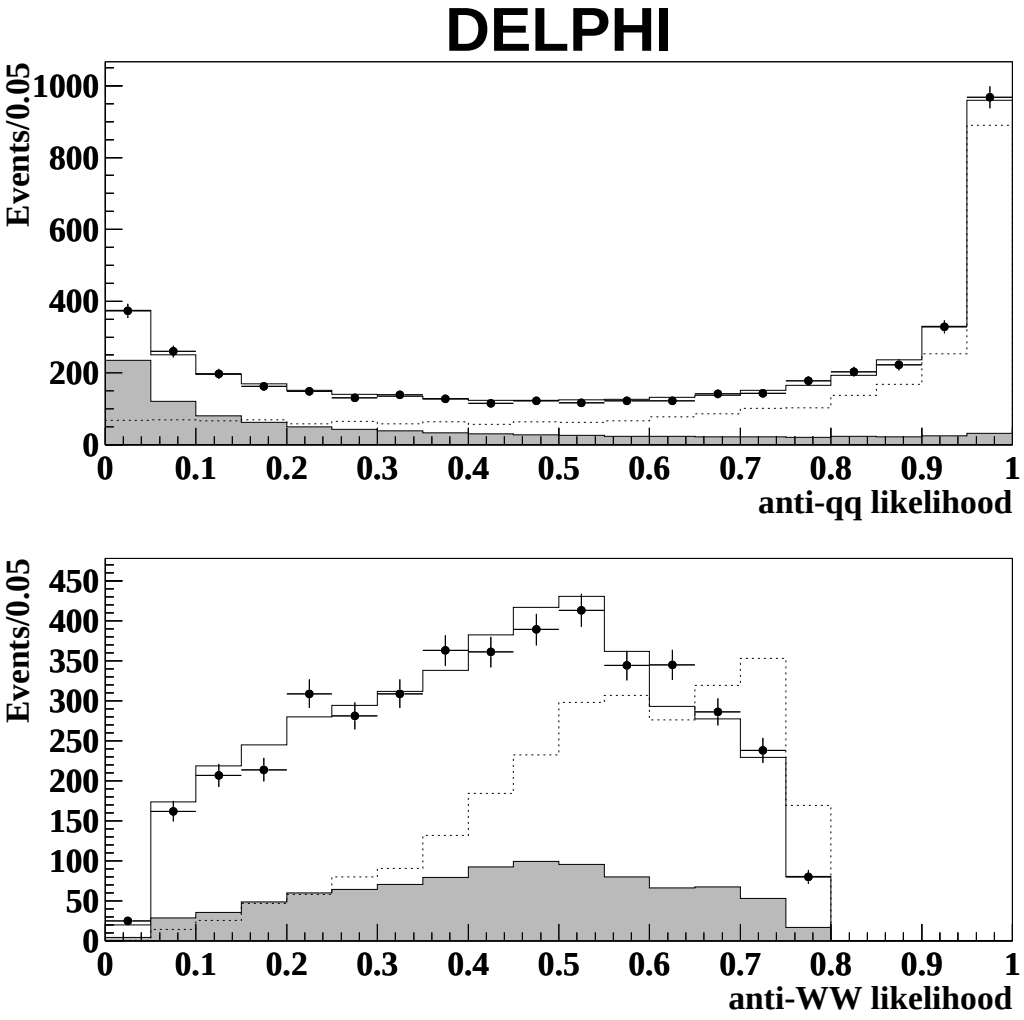

Figure 6: Distributions of the anti-qq and anti-WW likelihoods in the *cscs* analysis at 189–209 GeV. Data and expected SM backgrounds are indicated as in figure 5. The anti-QCD likelihood is plotted at the preselection level and the anti-WW likelihood after a cut on the anti-QCD likelihood. The expected distribution for a 75 GeV/c^2 charged Higgs boson signal is shown as a dotted histogram with arbitrary normalisation.

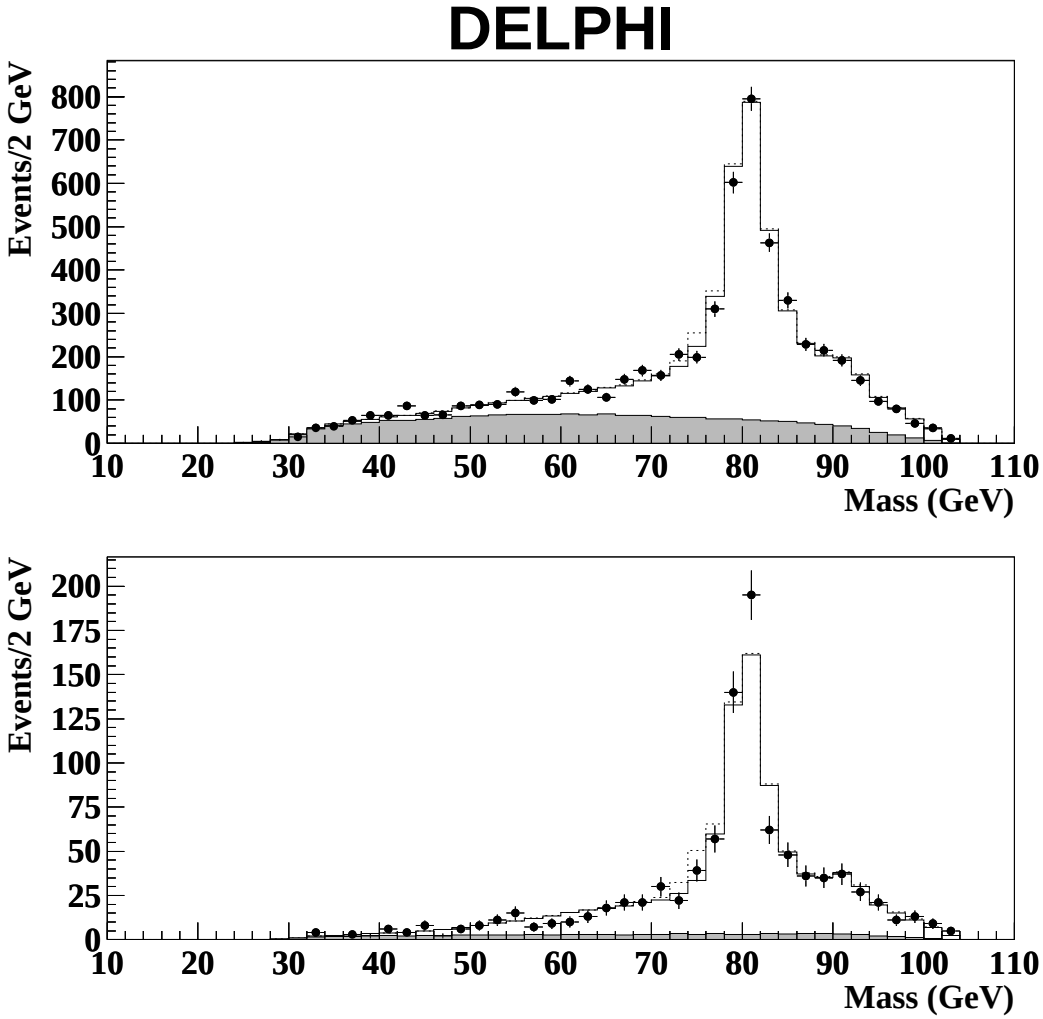

Figure 7: Reconstructed mass distribution in the *cscs* analysis at 189–209 GeV at preselection (top) and following the complete selection and requiring $\mathcal{L}$ ¿ 0.7 (bottom). The expected distribution in the presence of an H^+H^- signal, with $M_{H^\pm} = 75\text{GeV}/c^2$ and hadronic branching ratio of 100 %, is also shown for comparison (dotted).

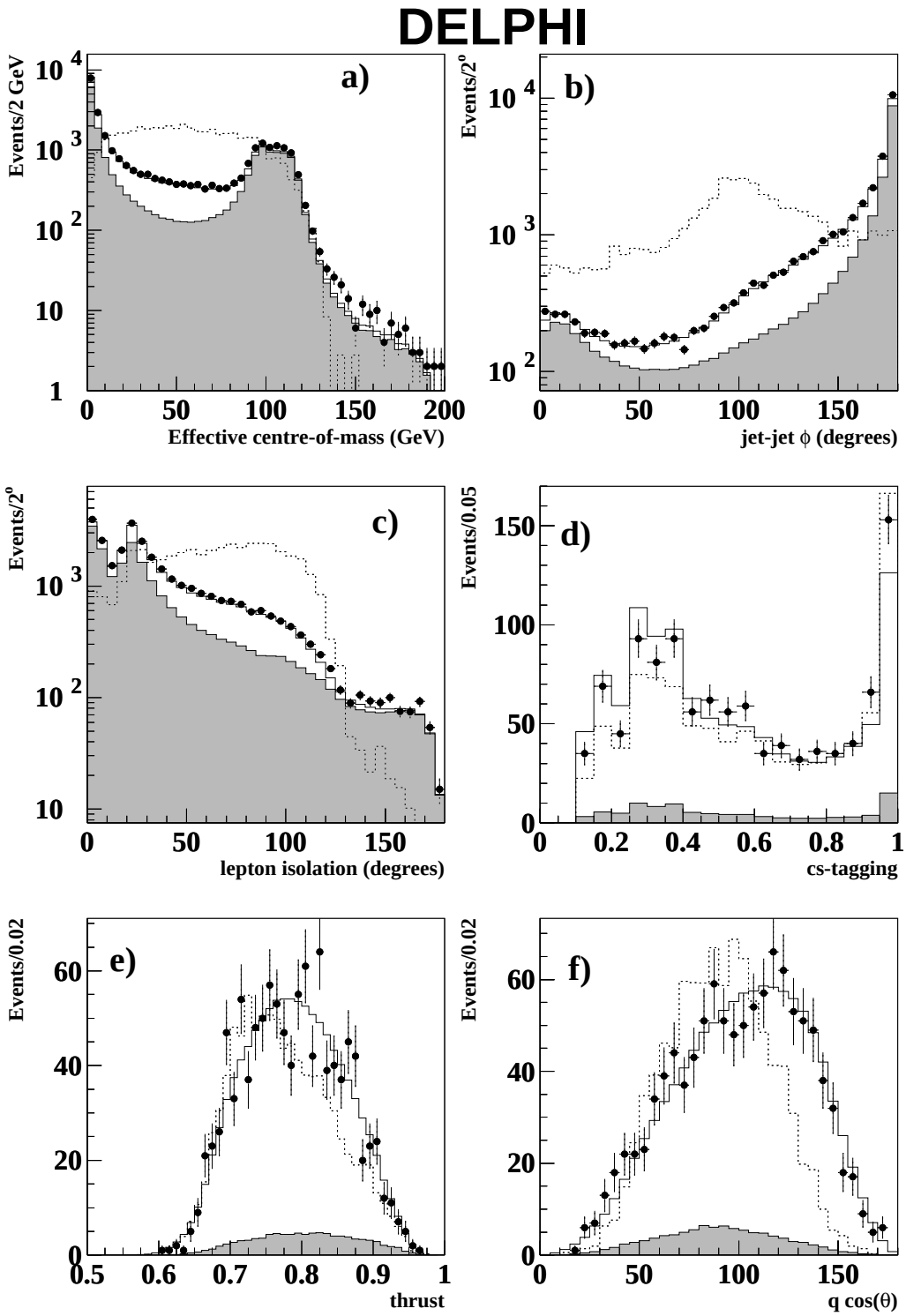

Figure 8: The distributions of some variables used in the $cs\tau\nu$ analysis. The effective centre-of-mass energy (a), the azimuthal angle difference of the jets (b), and the lepton isolation (c) were efficient against the $q\bar{q}$ background while the cs-tagging variable (d), the thrust (e), and the cosine of the polar angle (f) were used in the anti-WW likelihood. Data are shown as filled circles, while the solid histogram contour shows the expected SM background with contributions from WW (unfilled) and $q\bar{q}$ (shaded). The expected histogram for a 75 GeV/c^2 charged Higgs boson signal is shown as a dotted histogram with arbitrary normalisation for comparison.

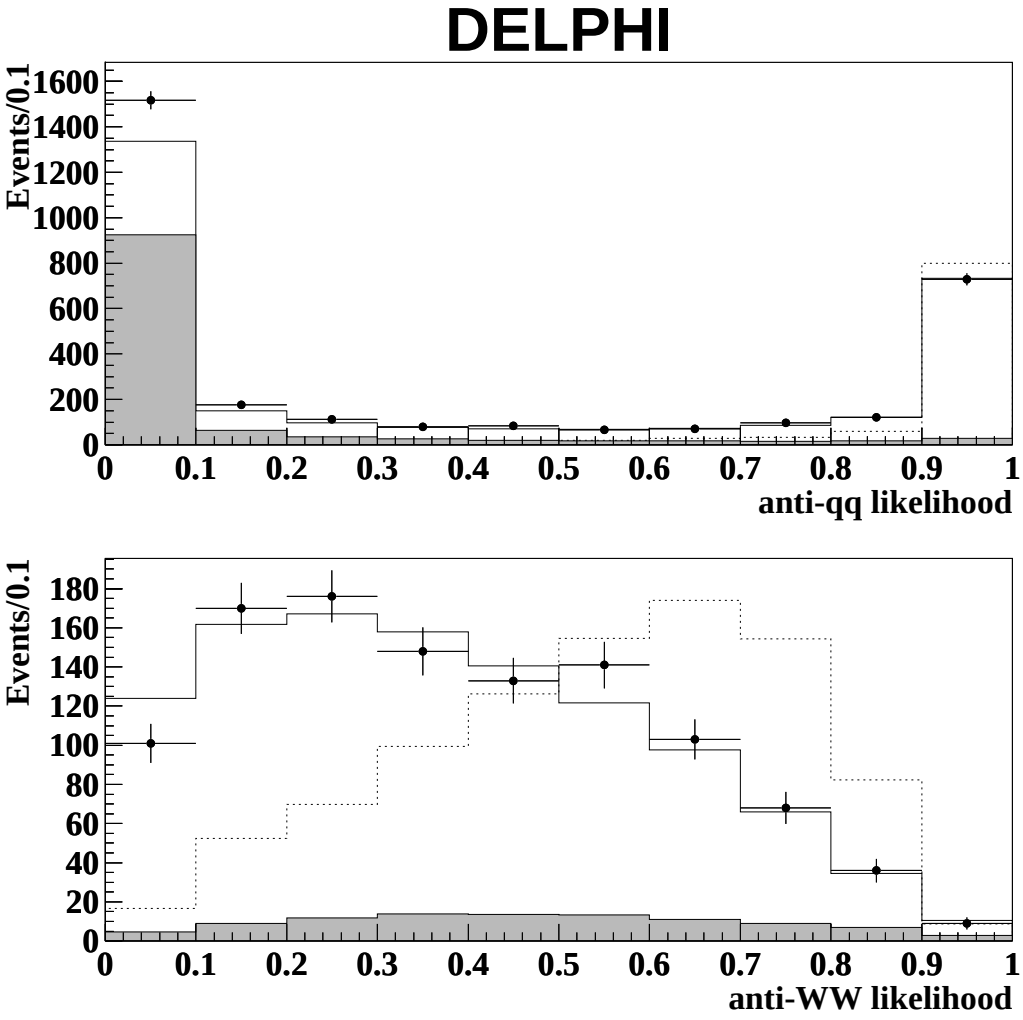

Figure 9: Distributions of the anti-qq and anti-WW likelihoods for the $cs\tau\nu$ analysis at 189–209 GeV. The anti-qq likelihood is plotted after applying all other cuts and the anti-WW likelihood at the final level. Data and SM background are indicated as in figure 8. The expected distribution for a 75 GeV/c^2 charged Higgs boson signal is shown as a dotted histogram with arbitrary normalisation.

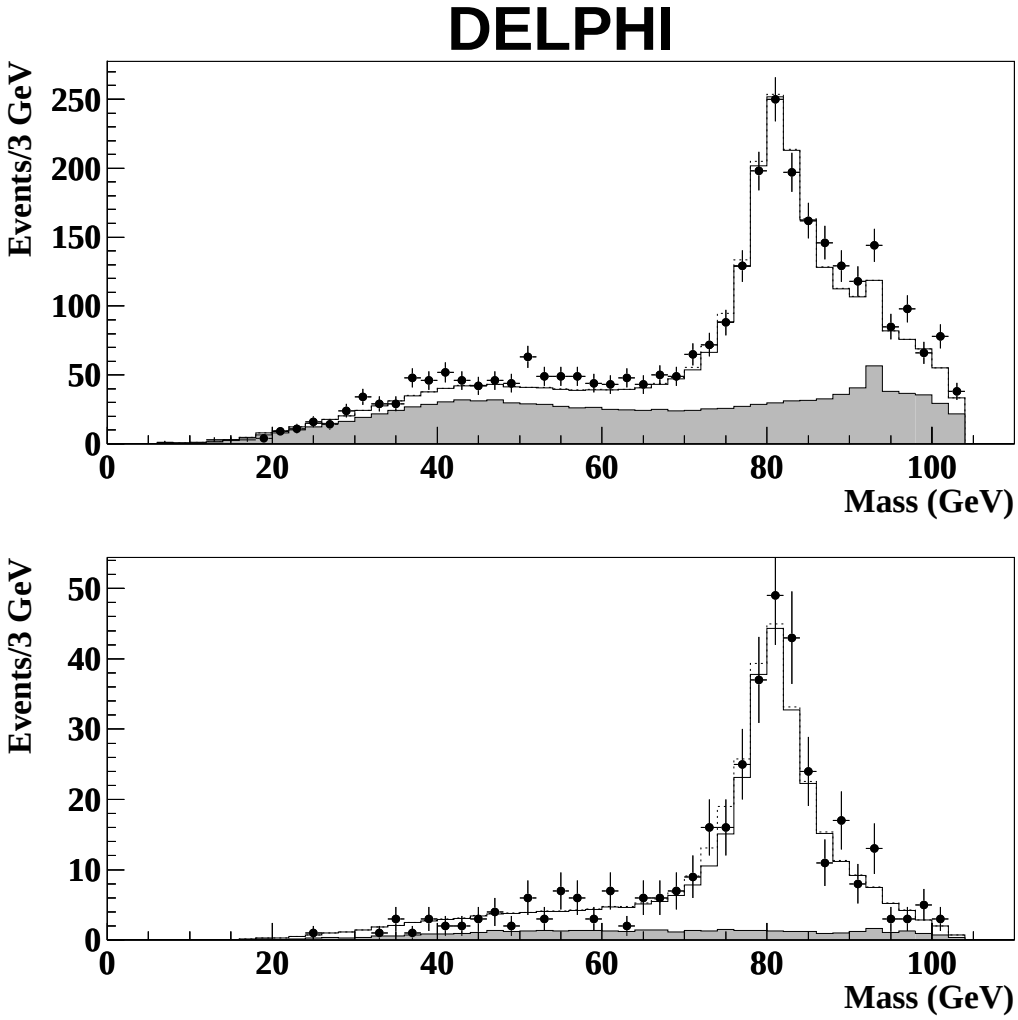

Figure 10: Reconstructed mass distribution in the $cs\tau\nu$ analysis at 189–209 GeV at preselection and at the final selection level, with a cut on the WW-likelihood $\mathcal{L}$ ¿ 0.5 . Data and SM background are indicated as in figure 8. The expected distribution in the presence of an H^+H^- signal, with $M_{H^\pm}$ = GeV/c^2 and leptonic branching ratio of 50 %, is also shown for comparison (dotted).

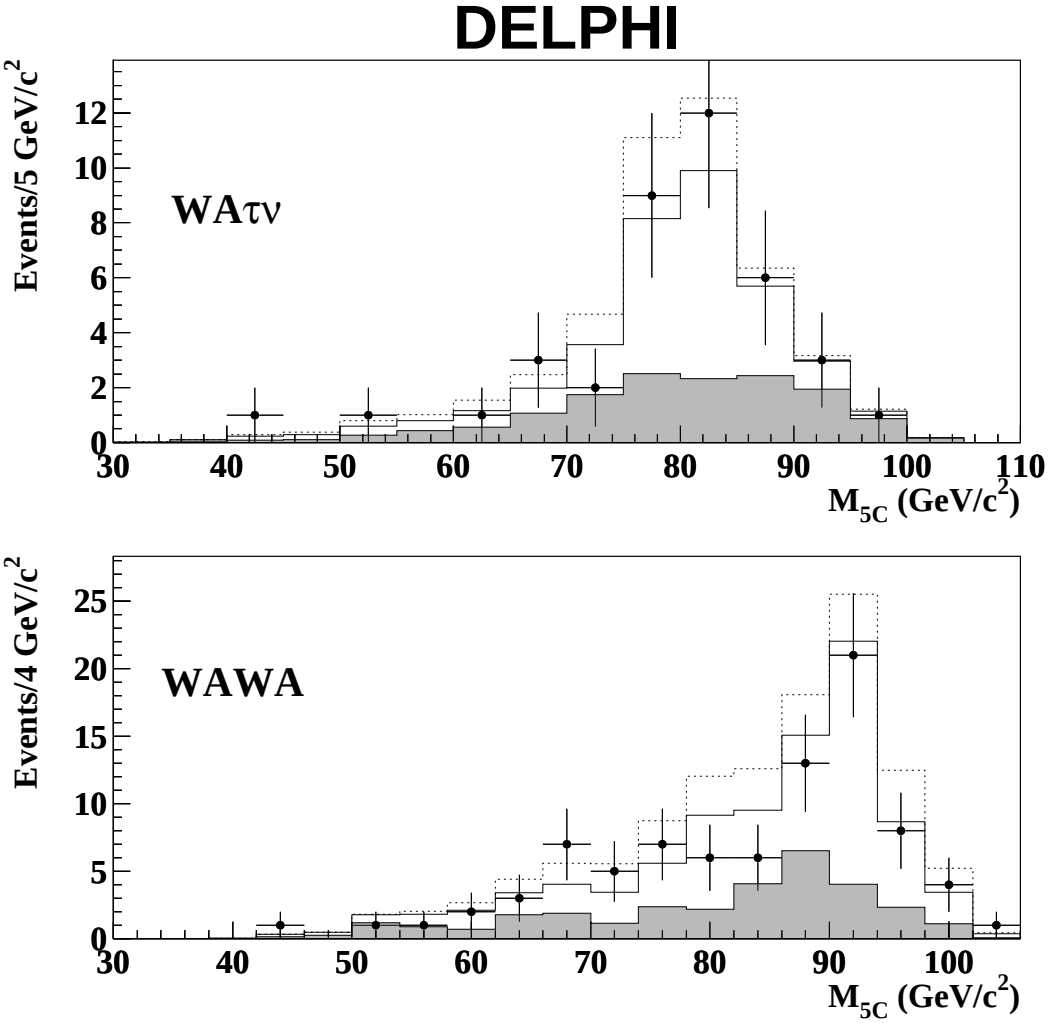

Figure 11: Reconstructed mass distribution of for events selected in the $W^*A\tau\nu$ (top) and W^*AW^*A (bottom) analyses by a cut on the neural network output of 0.1 and 0.3, respectively, for energies between 189–209 GeV. The data and the simulated SM background are indicated as in previous figures. The expected distribution in the presence of an H^+H^- signal, with $M_{H^\pm} = 80\text{GeV}/c^2$ and $M_A = 30$ GeV/c^2, is also shown for comparison (dotted).

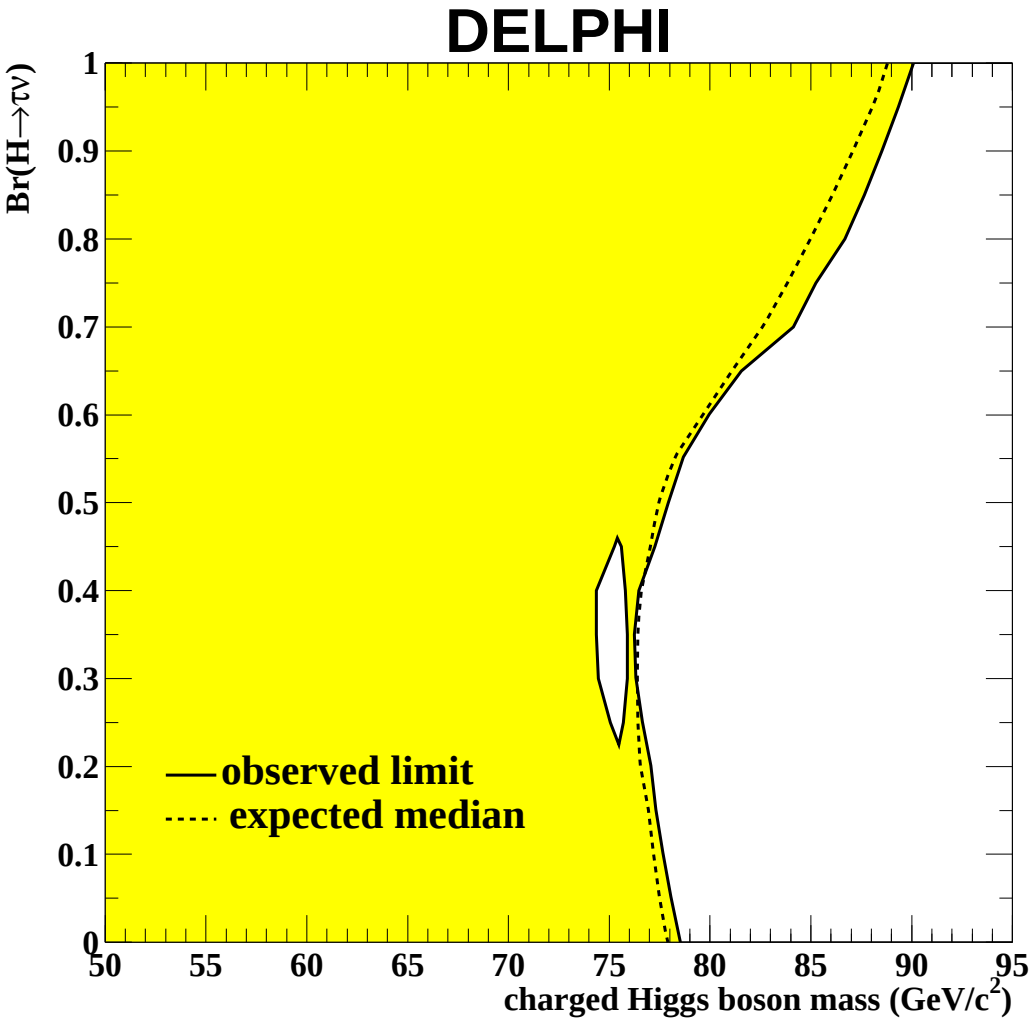

Figure 12: The observed and expected exclusion regions at 95% confidence level in the plane of BR($H \to \tau\nu_\tau$) vs. $M_{\mathrm{H}^\pm}$. These limits were obtained from a combination of the search results in the $\tau\nu\tau\nu$, $cs\tau\nu$ and $cscs$ channels at $\sqrt{s}$ = 183–209 GeV, under the assumption that the W^*A decay is forbidden.

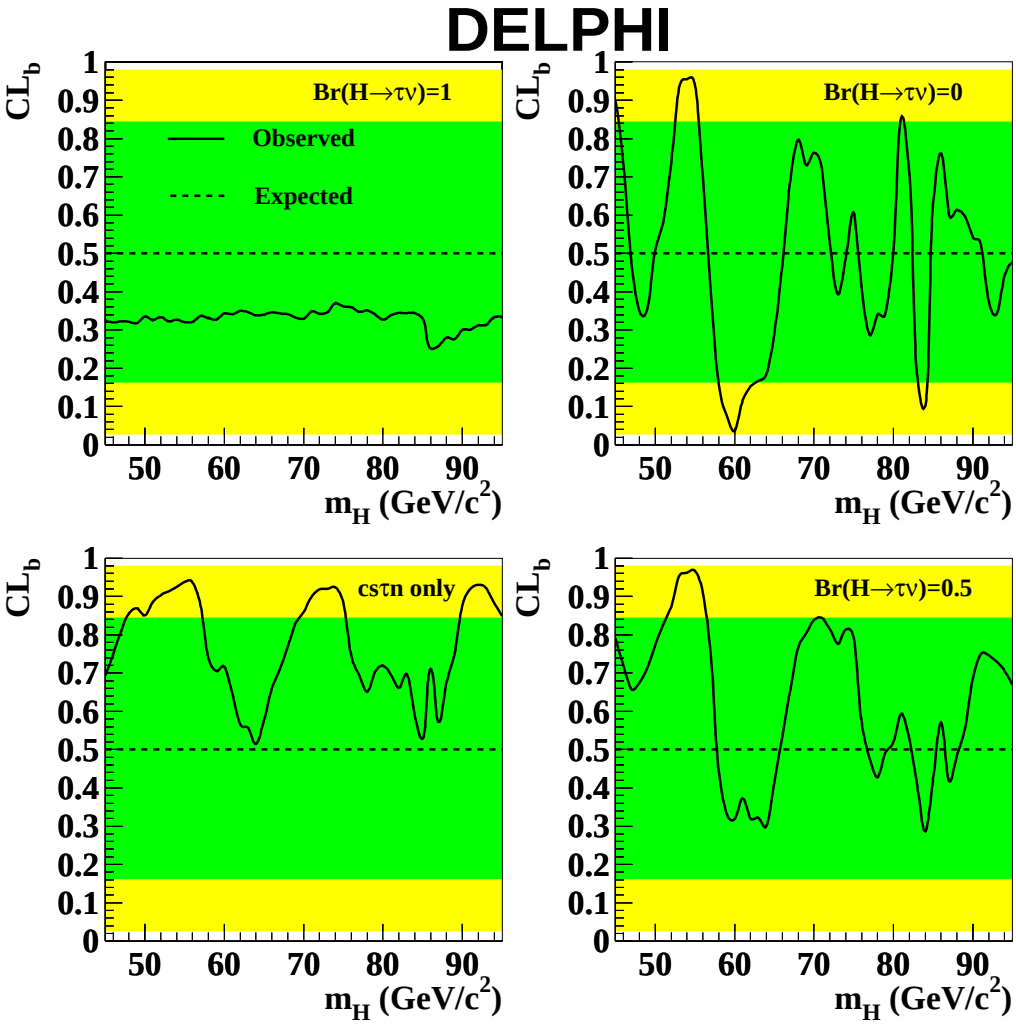

Figure 13: Confidence level for the background-only hypothesis for different branching ratios, under the assumption that the WA decay is forbidden. The full line shows the obtained CL_B and the horizontal dashed line at 0.5 indicates the expectation in the absence of a signal. The bands show the one and two standard deviation region for this expectation.

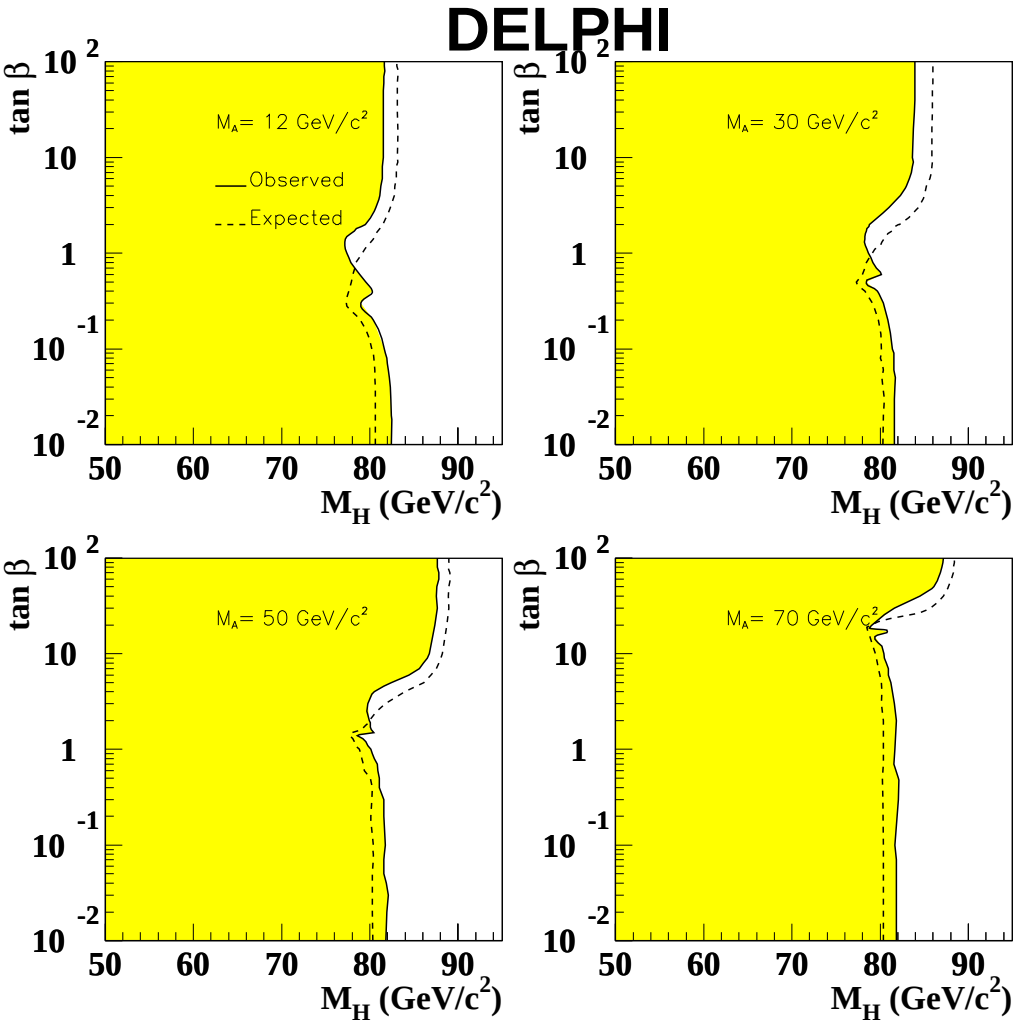

Figure 14: The observed and expected exclusion regions at 95% confidence level in the plane of $\tan\beta$ vs. $M_{\mathrm{H}^{\pm}}$. These limits were obtained from a combination of the search results in all five channels at $\sqrt{s} = 183$–209 GeV, for different A masses.

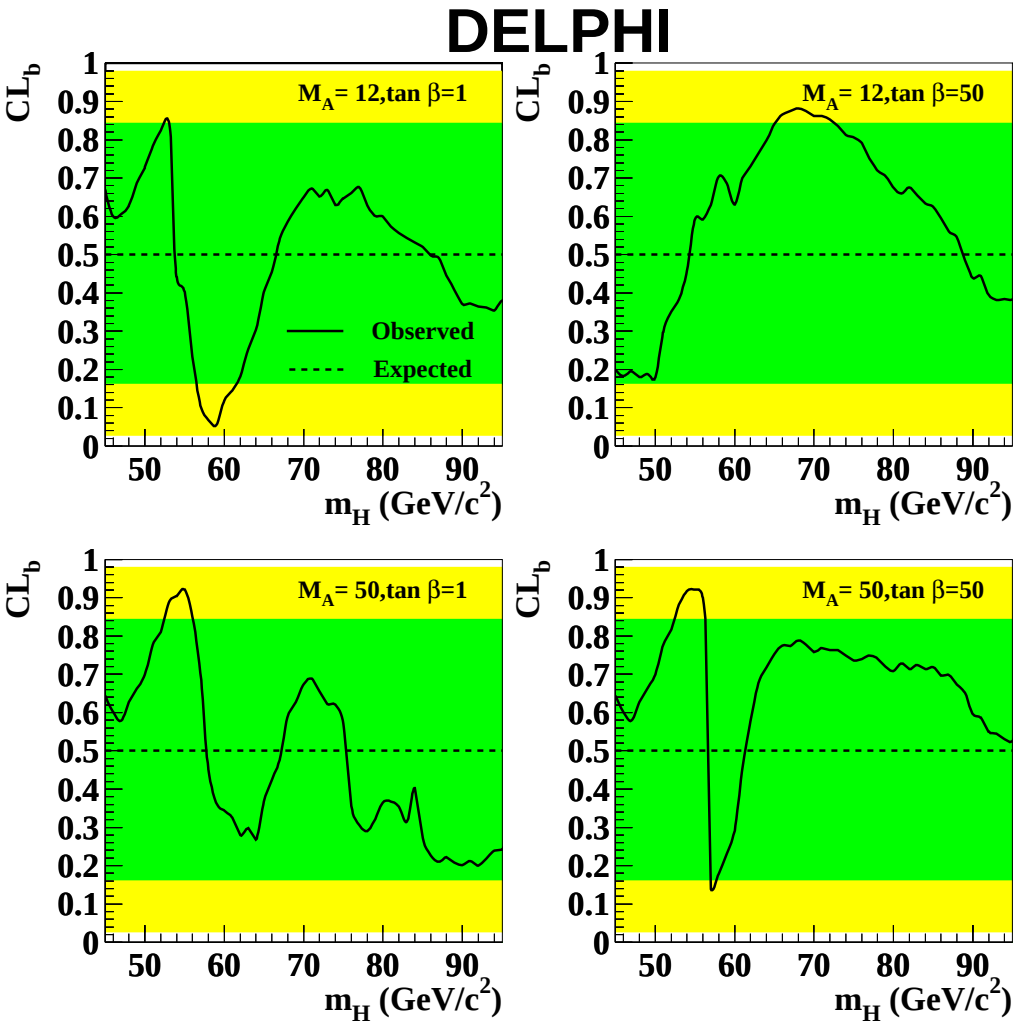

Figure 15: Confidence level for the background-only hypothesis for different $\tan\beta$ and A masses. The full line shows the obtained CL_B and the horizontal dashed line at 0.5 indicates the expectation in the absence of a signal. The bands show the one and two standard deviation region for this expectation.

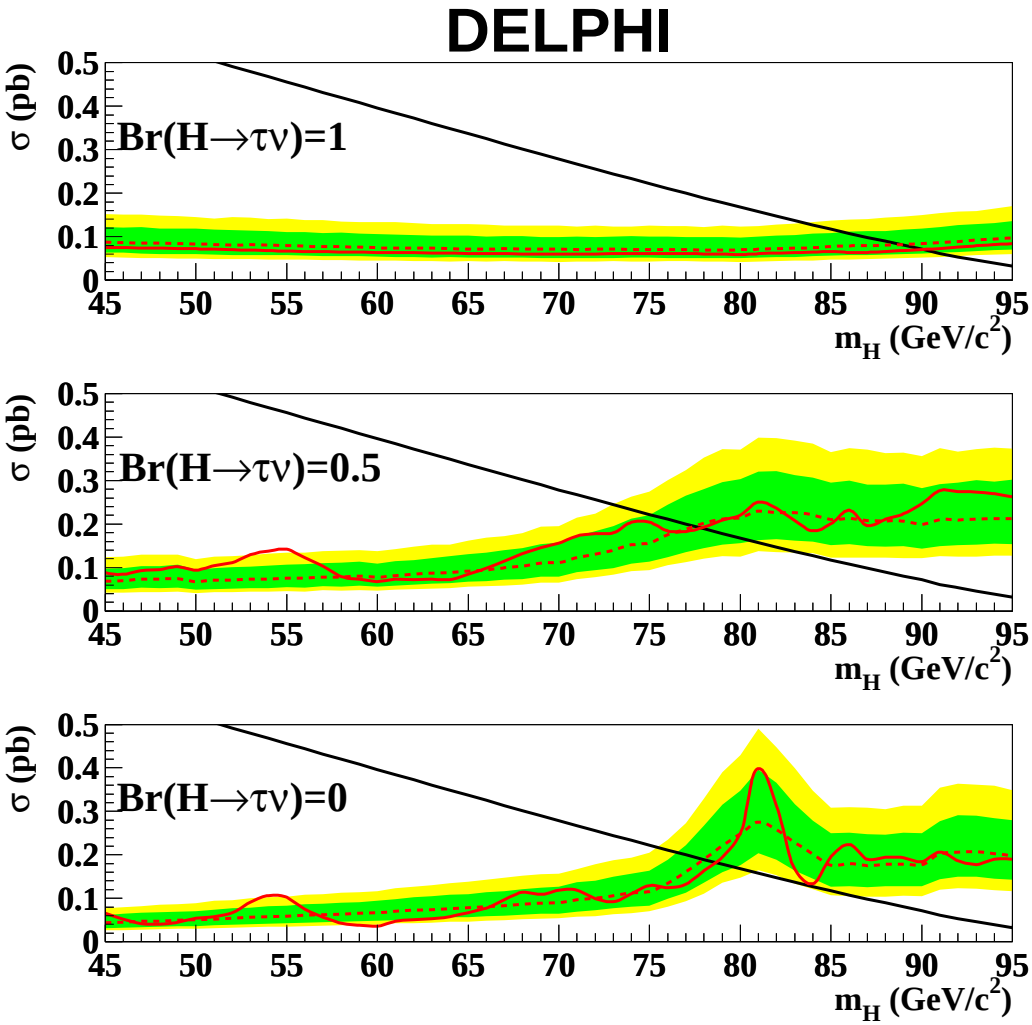

Figure 16: Upper limits on the cross-section for charged Higgs boson pair production at 95% confidence level, for different BR($H \to \tau\nu_\tau$), under the assumption that the W^*A decay is forbidden. The dashed curve shows the expected upper limit with one and two standard deviation bands and the solid curve is the observed upper limit of the cross-section. The solid black diagonal curve shows the 2HDM prediction. Cross-sections are given for 206.3 GeV centre-of-mass energy.

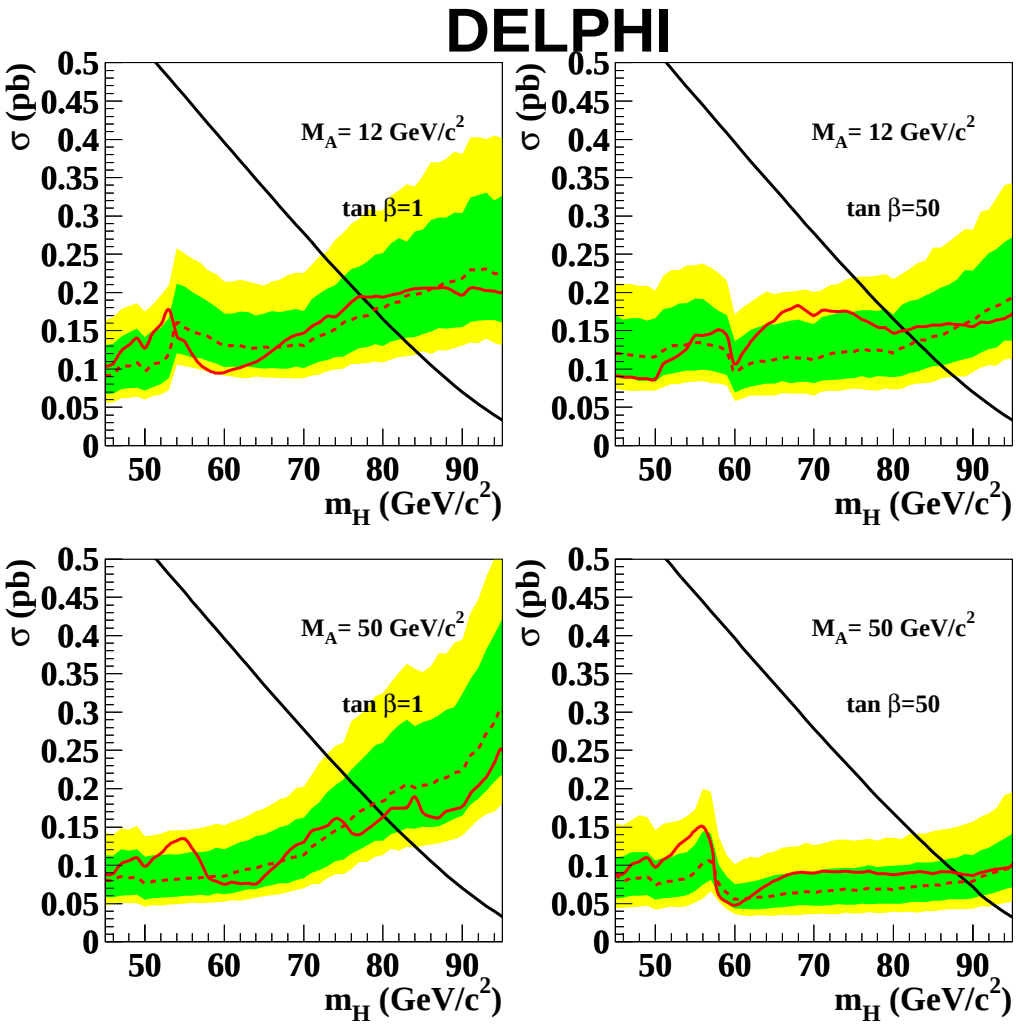

Figure 17: Upper limits, at 95% confidence level, on the production cross-section for a pair of charged Higgs bosons as a function of the charged Higgs boson mass, for different $\tan\beta$ and M_A and $\tan\beta$ values. The dashed curve shows the expected upper limit with one and two standard deviation bands and the solid curve os the observed upper limit of the cross-section. The solid black diagonal curve shows the 2HDM prediction. Cross-sections are given for 206.3 GeV centre-of-mass energy.